1. 研究課題名:

脳機能にリンクした局所酸素およびグルコース代謝のリアルタイム計測

2. 研究機関:

秋田大学

3. 研究者名と所属 :

山田勝也（秋田大学医学部生理学第一講座）

4, 研究協力者名と所属:

稲垣暢也（秋田大学医学部生理学第一講座）
堀本直幹（秋田大学医学部生理学第一講座）
中田正範（秋田大学医学部生理学第一講座）
松岡英明（東京農工大生命工学科生体機能工学講座）
Malonek, D.（Weizmann Institute, Israel）
Grinvald, A. （Weizmann Institute, Israel）
Dirnagl, U（Humboldt University, Germany）
Lindauer, U.（Humboldt University, Germany）
藤田英明(科学技術振興事業団秋田研究室)
松浦哲也(科学技術振興事業団秋田研究室)
菅野巌(秋田県立脳血管研究センター)

5. 研究期間:1996 年—1999 年

6. 要約

脳組織における酸素およびグルコース代謝を神経活動と共にリアルタイムに計測評価することを目標に、まず酸素に関してはヘモグロビンの酸素化脱酸素化と血流変化、更に神経活動を同時計測した。一方、グルコース取り込みを単一哺乳動物細胞でリアルタイムに観察する方法を確立し、更にグルコース取り込みに引き続く細胞機能と共に計測することに成功した。

7. 研究目的

近年、脳機能研究分野では PET、fMRI といった非侵襲的手法を駆使することで多くの新たな知見が蓄積されつつある。しかし、こうした近代的な手法は神経活動そのものではなく、脳活動を支える酸素代謝やグルコース代謝などを指標としているため、これら 2 次信号と神経活動との連関の詳細を明らかにすることが急務となっている。

特に、2 次信号と神経活動との相関の全体像を多角的に検討する上では、複数の二

次信号ならびに神経活動を生理学的条件下で同時に計測することが戦略のひとつとしてきわめて重要と考えられる。そこで我々はまず、1. 脳血流と局所酸素代謝という二つの因子を同時に観察すること。2. これらに加えて神経活動も測定すること。以上を目的として、その基本技術の確立を目指した。

一方、グルコース代謝に関しては、脳に限らずこれまでもっぱら放射性標識グルコースを利用して解析が行われてきた為、空間および時間分解能の制約により単一細胞レベルでの観察評価が困難で、このことがリアルタイムの研究を行う上で大きな妨げとなってきた。そこで今回我々は、新規蛍光標識 2-デオキシグルコース（2-NBDG）を用いる全く新たな手法を開発し、今後の脳におけるグルコース研究の新たな展開をはかる上での基礎的手法としての確立を目指した。

８．材料と方法

1）酸素消費のリアルタイム計測

実験には麻酔下のネコならびにラットを用いた。開頭後、密閉頭蓋チェンバーを装着し、脳血流をモニターするためにレーザードップラー（LDF)プローブを大脳皮質表面直上に挿入した。一方同時に、CCD カメラを用い、ヘモグロビンの酸素化脱酸素化に伴う光吸収の部位的ならびに時間的変化を定量した。ネコでは 8 方向のストライプ状の模様を用意し、コンピューターディスプレイ上に提示し、18 野にて記録した。ラットでは後肢を電気刺激して体性感覚野にて記録、またはひげを前後方向に機械刺激し、バレル野にて記録するとともに、観察部位の神経活動をモニターするためにガラス微小電極を刺入し、細胞外記録を行った。

2）グルコース輸送のリアルタイム計測

新規に合成した蛍光指示 D-glucose 誘導体 2-[*N*-(7-nitrobenz-2-oxa-1, 3-diazol-4-yl)amino]-2-deoxy-D-glucose (2-NBDG)をグルコースプローブとして用いた。ほ乳動物細胞に対する 2-NBDG の取り込みをみることを目的として COS-1 細胞にグルコーストランスポータ GLUT1,2,3 を過剰発現させたものを用いた。またグルコース取り込みのカイネティクスの詳細が明らかとなっている細胞としてインスリノーマ由来の MIN6 細胞を用いた。さらに、ネイティブの細胞としてラット膵ランゲルハンス島細胞を常法に従って単離して用いた。倒立蛍光顕微鏡下、細胞を Krebs Ringer 液にて潅流しながら、励起波長 465-495nm、吸収は 520-560nm にて Silicon-intensified target camera を用いて観察した。一方、細胞活動をモニターするため、細胞内 Ca2+イオン指示薬として Fura-2 を用い、340nm と 380nm の吸光度の比を Argus50（浜松ホトニクス）にて計測した。

９．結果

1）局所酸素消費と神経活動ならびに局所血流変化のリアルタイム計測

まず脳賦活時の酸素消費と血流変化との関係を調べるために、ネコに視覚刺激を加え、大脳皮質視覚野にて記録を行った。今回、われわれは局所の神経活動に伴って生じる血流変化を LDF 法により計測すると同時に、ヘモグロビンの酸素化脱酸素化を光信号により同時にとらえることに初めて成功した。その結果、LDF により求められた局所脳血流の変化は、内因性シグナルの光学的記録法により調べられた脱酸素化（605nm における吸収）より 1 秒以上遅れて生じることなどが明らかとなった。この結果は、毛細血管床の血液量をコントロールする積極的な神経血管調節メカニズムの存在を支持している（Fig. 1; Malonek, et al., 1997)。

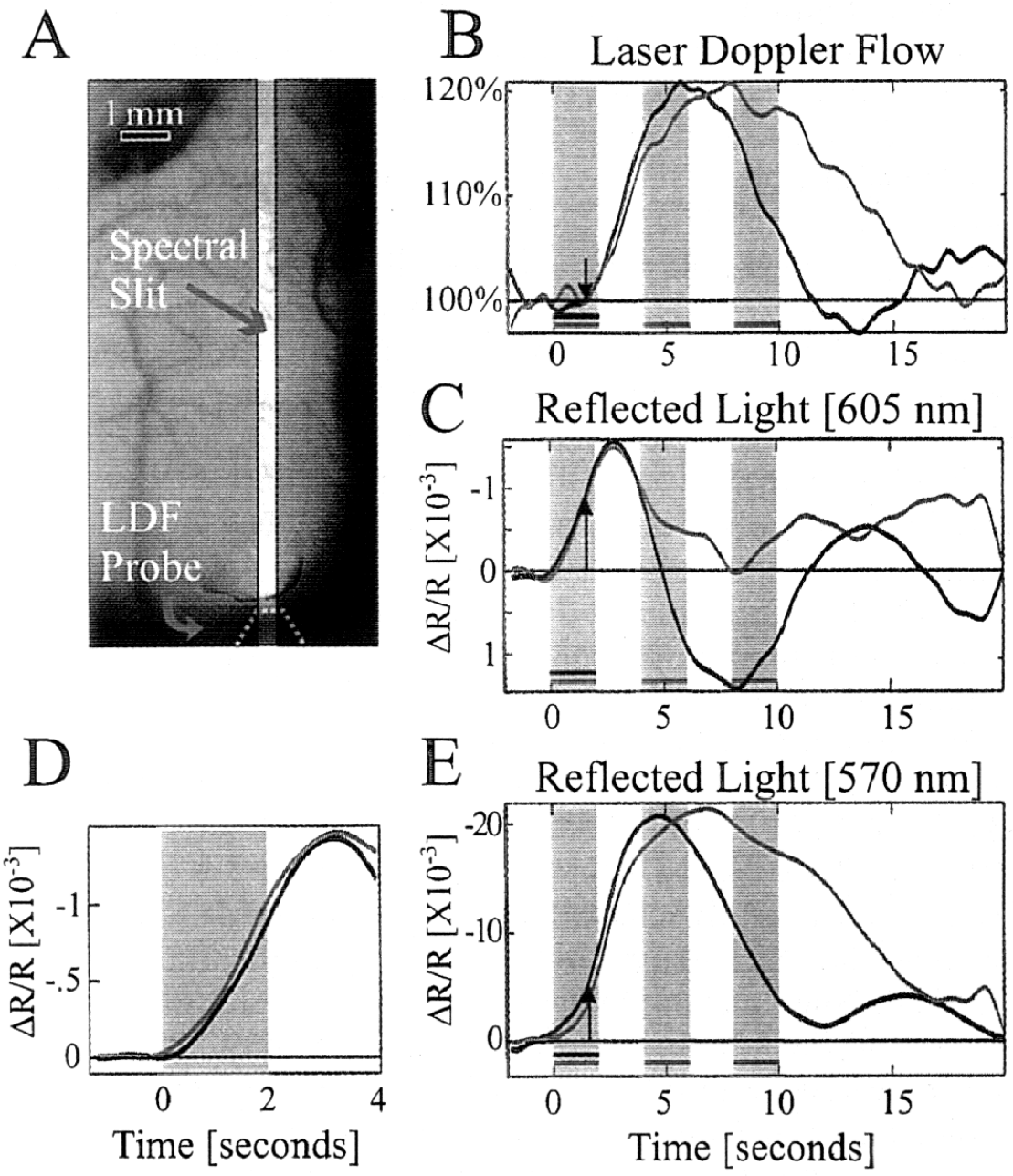

Fig.1 皮質の内因性光信号反射と皮質血流の同時記録

A, 皮質表面のイメージ。B, レーザードップラー血流反応。→で示された立ち上がりは約 1.5sec 刺激より遅れている。C, 605nm における反射で、その立ち上がりは LDF より 1sec 先行している。太く濃い線は短い（2sec）刺激に対する応答で、薄い線は長い（10sec）刺激に対するものである。D, 605nm における反応の初期相。E, 570nm における反射。

一方、神経活動と皮質血流量の変化との関係について直接調べた研究もきわめて少なく、不明の点が多い。そこで、ラットの後肢を電気刺激し、大脳皮質体性感覚野に生じた神経活動を測定し、同時に LDF により、興奮部位の皮質血流変化を計測した。

その結果、神経活動時の皮質赤血球濃度変化、血流速度変化、ならびに流束（Flux）変化はほぼ同時に始まるが、赤血球濃度のピークは、血流速度ならびに Flux のピークより早く生じることなど、相互の時間的関係が明らかとなった。この結果は、抵抗血管である細動脈の変化だけでは説明しにくく、毛細血管のアクティブな変化が介在している可能性を示唆するものである（Matsuura, et al., 1999)。

上記の記録は、血流変化、ヘモグロビンの酸素化などを神経活動と同時に調べようとするものであるが、従来これら３つを同時に観察することは困難と考えられていた。また、脳硬膜を破る方法では頭蓋内圧の一時的破綻が脳血管調節メカニズムに与える影響に不安が残り、硬膜を保存する方法では観察の空間分解能が不十分というジレンマがあった。そこで、われわれは新規密閉頭蓋チェンバーの開発により、術中、実験中を含めて頭蓋内圧を生理学的範囲に維持して血管反応性を観察するとともに、上記 3 者を同時記録することに初めて成功した（Fujita, et al., 2000)。

2）哺乳動物細胞内へのグルコース輸送のリアルタイム観察ならびに細胞機能の同時評価

哺乳動物細胞内へのグルコース輸送は促通拡散型グルコーストランスポータを通じて行われることが知られており、現在 GLUT1-5 の 5 種類がクローニングされている。そこでまず代表的な低親和性トランスポーターである COS-1 細胞に GLUT2 を過剰発現させた上、2-NBDG（200μM）投与前後で蛍光強度の変化を観察した。その結果、GLUT2 過剰発現細胞では蛍光強度が大きく変化し、2-NBDG の取り込みがみられたが、対照細胞では有意な変化が認められなかった。また 2-NBDG の取り込みの定量的評価を行うために大量の GLUT2 を発現している MIN6 細胞を用いた。その結果、2-NBDG の MIN6 細胞に対する取り込みは 25℃では 37℃の約半分で、かつ時間依存的に増大し、GLUT 阻害剤であるサイトカラシン B（10μM）により完全に阻害された。また 2-NBDG 取り込みは D-グルコースによっても濃度依存的に阻害された。更に 2-NBDG 取り込みの Km 値は MIN6 細胞に発現する GLUT を介した D-グルコース取り込みの文献値に一致した。同様の結果は　GLUT1 および 3 でもみられ、これらの結果から 2-NBDG は哺乳動物細胞にグルコーストランスポータを介して特異的に取り込まれることが示された (Fig. 2; Yamada, et al., 2000)。

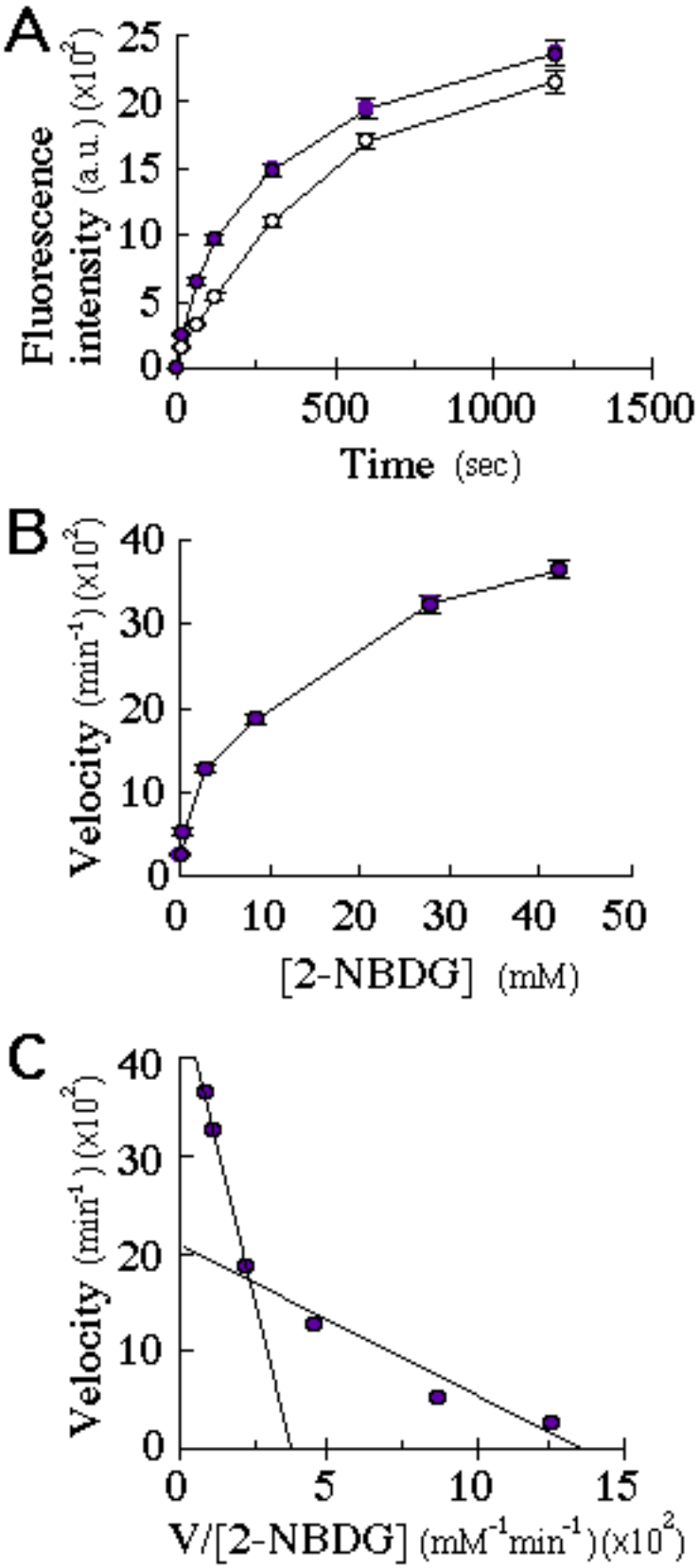

Fig. 2 2-NBDG の MIN6 細胞への取り込みの定量的解析。

A, 2-NBDG の投与時間に対する蛍光強度の変化。B, 2-NBDG 濃度に対する反応速度の関係。C, B により計算された Eadie-Hofstee plot で、二つの曲線から 2-NBDG 取り込みの Km 値は 13.3 および 1.6

となり、それぞれグルコースの GLUT2 および 1 に対する取り込みの文献値に匹敵する。

次にグルコース取り込みと細胞機能との関係を同一細胞において評価することを試みた。もっともグルコース取り込みによって引き起こされる細胞機能のよく調べられている細胞の一つとして、ラット膵臓から単離した単一ラ氏島細胞を対象として、グルコース取り込みを 2-NBDG により、インスリン分泌に伴う細胞内カルシウムイオン濃度（$[Ca^{2+}]_i$）の変化を fura-2 により解析した。その結果、全てのインスリン陽性膵β細胞は、2-NBDG（200 M）投与により有意な取り込みを示した。高グルコース刺激に対しては$[Ca^{2+}]_i$上昇を示す細胞と示さない細胞が存在し、ミトコンドリアの脱共役剤ジニトロフェノール（50 M）はこの$[Ca^{2+}]_i$上昇を阻害したが、2-NBDG 取り込みには影響しなかった。他方、グルカゴン陽性α細胞は、有意な 2-NBDG 取り込みを示さず、高グルコース刺激にも応答しなかった。2-NBDG を長時間（10min）投与するとα細胞にも取り込まれるが、その量はβ細胞の 1/10 以下であった。これらの結果により、膵β細胞はα細胞に比較してグルコース取り込みがはるかに大きく、またそのインスリン分泌に伴う$[Ca^{2+}]_i$上昇には、グルコース取り込みと同時にグルコースの細胞内代謝が重要であることが示唆された(Yamada, et al., ibid)。

10．考察

脳賦活時の局所酸素消費と局所血流変化との関係を脳実質内において同時に調べた研究はこれまでになく、今回の結果は、従来不明であった両者の時間的関係について測定した初めての報告と考えられる。また、これら血流変化およびヘモグロビンの酸素化の両者にくわえて、更に局所神経活動を同時に観察することは技術的に困難と考えられていた。しかし、今回我々はこれら 3 者の同時計測が可能であることを明確に示した。また、本手法はレーザードップラー血流計と、内因性光シグナルの組み合わせだけでなく、その他の異なる複数の測定手段を組み合わせることで、きわめて多くの応用が可能である。

第二に、本実験では従来ややもすれば軽視されたり、不十分であった麻酔管理を血液ガスのモニターしながら厳密に行った。また術中術後を含めて頭蓋内圧を生理的範囲に一定に保つ方法を確立したことで、正常な血管反応性を維持したままこれらの詳細な測定を行うことが可能になった。血管反応性といった観点からこのことはきわめて重要な意味を持ち、こうした手法から得られる結果は、神経活動と二次信号との関連が正常な生理学的条件下でどのように変化するかという問題に対して有力な情報を提供するものと思われる。

今回我々は、脳におけるグルコース輸送を解析する上で、従来の放射性標識グルコ

ースを用いる方法にかわる新たな手法として新規蛍光標識 2-デオキシグルコース 2-NBDG を用いることが可能であることを示した。2-NBDG によるグルコース輸送の研究は一般のどの研究室でも備えているような比較的小規模の顕微鏡設備を用いておこなうことができる。しかも強力な蛍光を発するため感度はきわめて鋭敏で、更に単一細胞レベルでの今回の結果にもみられるように時間的空間的分解能のいずれにおいても優れている。2-NBDG はきわめて高濃度で長時間用いた場合には、グルコース輸送量と蛍光強度との直線性がずれてくることも考えられる。しかし、今回記述したように適切な濃度ならびに投与時間を用いることで、2-NBDG はグルコース研究において全く新しい角度からの情報を与えてくれるものと期待される。

11．今後の展開

本実験ではヘモグロビンの酸素化脱酸素化を利用した光シグナルの変化を利用して酸素代謝を評価した。脳実質内の酸素分圧変化をより直接的に調べる手法の一つとしては、今後酸素電極を本手法と併用することが考えられる。これにより従来議論のあった内因性光シグナルの解釈に関しても一歩進んだ解釈を与えることができる可能性がある。

また、その他にも本システムでは電極法で測定可能なカリウム、pH、各種代謝産物といった神経活動に伴って脳内で大きく変化する因子のダイナミックスを、各種光信号に基づく２次元的観測と併用できる。これらの利点を生かせば、時間的に変化する生理学的反応を脳の比較的広い範囲において、十分な組織学的空間解像度をもってリアルタイムに観察することも可能になる。以上の観点から本手法は人を用いた PET や MRI 研究と細胞レベルのリンクとしても有望であるものと期待される。

蛍光標識 2-デオキシグルコース 2-NBDG による測定は、脳スライスなど組織レベルの研究や in vivo 研究に対する応用可能性があり、実際我々も予備的実験を開始していくつかの結果を得ている。また細胞組織レベルに留まらず、コンフォーカル顕微鏡と組み合わせることで細胞内のグルコース局在や移動、その時間経過の研究においても有用である。現在脳内エネルギー代謝研究のもっともホットな問題の一つに脳神経活動を支える直接のエネルギーソースがグルコースであるかどうかという議論があり、蛍光標識グルコースがこの分野に新たな観点から貢献できるのではないかと期待される。

12．参考文献

13．研究業績

13-1.原著論文：

[1] D. Malonek, U. Dirnagl, U. Lindauer, K. Yamada, I. Kanno and A. Grinvald: Vascular imprints of neuronal acitvity: Relationships between the dynamics of cortical blood flow, oxygenation, and volume changes following sensory stimulation. *Proc. Natl. Acad. Sci. USA*, 94, 14826-14831 (1997).

[2] T. Matsuura, H. Fujita, C. Seki, K. Kashikura, K. Yamada, and I. Kanno: CBF Change evoked by somatosensory activation measured by laser-Doppler flowmetry: Independent evaluation of RBC velocity and RBC concentration. *Jpn. J. Physiol.* 49, 289-296 (1999).

[3] K. Yamada, M. Nakata, N. Horimoto, M. Saito, H. Matsuoka and N. Inagaki: Measurement of glucose uptake and intracellular calcium concentration in single, living pancreatic -cells *J. Biol. Chem*, 275, 22278-22283 (2000).

[4] H. Fujita, T. Matsuura, K. Yamada, N. Inagaki and I. Kanno: A sealed cranial window system for simultaneous recording of blood flow, electrical and optical signals in the rat barrel cortex. *J. Neurosci. Meth.* (in press).

13-2.総説など：なし

13-3.国際学会発表：

[1] D. Malonek, U. Dirnagl, I. Kanno, K. Yamada and A. Grinvald: Correlation of blood flow and blood oxygenation changes in functionally activated cat visual cortex, 18th. International Symposium on Cerebral Bloodflow and Metabolism (Brain 97), June 15-19, 1997, Baltimore.

[2] N. Horimoto, K.Yamada, N. Okada: Observation of the three-dimensional structure of subsurface blood vessels in rat cerebral cortex in vivo using ultrasound microscopy, 27th Annual Meeting, Society for Neuroscience, October 25-30, 1997, New Orleans.

[3] T. Matsuura, H. Fujita, C. Seki, K. Kashikura, K. Yamada and I. Kanno: Local CBF change evoked by hind paw stimulation measured using LDF in rat brain. 28th. Annual Meeting Society for Neuroscience, November, 7-12, 1998, Los Angeles.

[4] H. Fujita, T. Matsuura, K. Yamada, and I. Kanno: A chamber system for simultaneous recording of electrical, blood flow and optical signals of rat barrel cortex. 28th. Annual Meeting Society for Neuroscience, November,

7-12, 1998, Los Angeles.

13-4.国内学会発表：

[1] 松浦哲也、藤田英明，関千江，柏倉健一，山田勝也，菅野巌：ラット後肢電気刺激に対する大脳皮質体性感覚野の興奮と局所脳血流量の変化、第 69 回日本動物学会、平成 10 年 9 月 26 日、広島。

[2] 堀本直幹、山田勝也、中田正範、稲垣暢也：蛍光指示 2-デオキシグルコースを用いた単一細胞におけるグルコース取り込みの観察、第 31 回東北生理談話会、平成 10 年 10 月 24 日、山形。

[3] 山田勝也、堀本直幹、中田正範、松岡英明、稲垣暢也：蛍光指示 2-デオキシグルコースを用いた単一細胞におけるグルコース取り込み、第 76 回日本生理学会、平成 11 年 3 月 28-30 日、長崎。

[4] 中田正範、山田勝也、松岡英明、稲垣暢也：蛍光指示 2-デオキシグルコースを用いた膵島細胞のグルコース取り込み・機能連関、第 42 回日本糖尿病学会学術集会、平成 11 年 5 月 13 日、横浜

14. Real-time measurements of local oxygen and glucose metabolism that link to the brain function

15. Akita University School of Medicine

16. Katsuya Yamada (Department of Physiology, Akita University School of Medicine)

17.

Nobuya Inagaki (Department of Physiology, Akita University School of Medicine)

Naoki Horimoto (Department of Physiology, Akita University School of Medicine)

Masanori Nakata (Department of Physiology, Akita University School of Medicine)

Hideaki Matsuoka (Department of Biotechnology, Tokyo University of Agriculture and Technology)

Malonek, D.（Weizmann Institute, Israel）

Grinvald, A. （Weizmann Institute, Israel）

Dirnagl, U（Humboldt University, Germany）

Lindauer, U.（Humboldt University, Germany）

Hideaki Fujita (JST Akita)

Testuya Matsuura (JST Akita)
Iwao Kanno (Akita Research Institute of Brain and Blood Vessels)

18. 1996-1999

19. Abstract

Under a photic or somatosensory stimulation, we simultaneously measured local redox state of hemoglobin and local blood flow changes at visual and somatosensory cortex. A laser-Doppler flowmetry were used for the blood flow measurement. The results suggest time-course in the onset of local blood flow increase was delayed over 1 sec after changes in the deoxygenation of hemoglobin. In addition, we established a basic technique to measure the relationship between neuronal activity and the secondary signal by using multiple different measurements simultaneously.

By using a novel fluorescent 2-deoxyglucose, 2-NBDG as a tracer for glucose transport, we have made a real-time monitoring of glucose uptake into single, mammalian cells possible. Furthermore, by use of Fura-2, an intracellular calcium indicator, together with 2-NBDG measurement. This first enabled to estimate directly both glucose-uptake and concomitant cellular functions in the same cell.

Proc. Natl. Acad. Sci. USA
Vol. 94, pp. 14826–14831, December 1997
Neurobiology

Vascular imprints of neuronal activity: Relationships between the dynamics of cortical blood flow, oxygenation, and volume changes following sensory stimulation

(hemodynamics/blood oxygenation/laser Doppler flowmetry/cerebral microcirculation/optical imaging)

DOV MALONEK*†, ULRICH DIRNAGL‡, UTE LINDAUER‡, KATSUYA YAMADA§, IWAO KANNO¶, AND AMIRAM GRINVALD*

*Department of Neurobiology, Weizmann Institute of Science, Rehovot 76100, Israel; ‡Experimental Neurology, Department of Neurology, Charité Hospital, Humboldt University, Berlin, Germany; §Department of Physiology, Akita University School of Medicine, Akita, 010 Japan; and ¶Department of Radiology and Nuclear Medicine, Akita Research Institute of Brain and Blood Vessels, Akita, 010 Japan

Communicated by Louis Sokoloff, National Institutes of Health, Bethesda, MD, October 24, 1997 (received for review June 9, 1997)

ABSTRACT **Modern functional neuroimaging methods, such as positron-emission tomography (PET), optical imaging of intrinsic signals, and functional MRI (fMRI) utilize activity-dependent hemodynamic changes to obtain indirect maps of the evoked electrical activity in the brain. Whereas PET and flow-sensitive MRI map cerebral blood flow (CBF) changes, optical imaging and blood oxygenation level-dependent MRI map areas with changes in the concentration of deoxygenated hemoglobin (HbR). However, the relationship between CBF and HbR during functional activation has never been tested experimentally. Therefore, we investigated this relationship by using imaging spectroscopy and laser-Doppler flowmetry techniques, simultaneously, in the visual cortex of anesthetized cats during sensory stimulation. We found that the earliest microcirculatory change was indeed an increase in HbR, whereas the CBF increase lagged by more than a second after the increase in HbR. The increased HbR was accompanied by a simultaneous increase in total hemoglobin concentration (Hbt), presumably reflecting an early blood volume increase. We found that the CBF changes lagged after Hbt changes by 1 to 2 sec throughout the response. These results support the notion of active neurovascular regulation of blood volume in the capillary bed and the existence of a delayed, passive process of capillary filling.**

There is a tight coupling between electrical activity in the brain and both cellular metabolism and hemodynamic changes, as shown in the pioneering work of Roy and Sherrington (1), Ketty and Schmidt (2), Sokoloff *et al.* (3), and Chance *et al.* (4). This coupling is used by modern, functional neuroimaging methods, like positron-emission tomography (PET) (5, 6), optical imaging (7, 8), and functional MRI (fMRI) (9–11) to obtain, indirectly, maps of neuronal activity. These imaging techniques rely on various types of activity-dependent changes: regional changes in cerebral blood flow (CBF) were first used for functional mapping of the brain by PET studies and subsequently by single photon emission computed tomography (SPECT) and by flow-sensitive MRI. The optical imaging technique relies on color changes associated with either cerebral blood oxygenation changes or blood volume changes (CBV) and produces maps of the functional architecture of the cortex at a spatial resolution even higher than that needed to resolve individual functional domains (7, 8). These high-resolution optical maps provide evidence for a very precise spatial match between cortical electrical activity and localized changes in blood deoxyhemoglobin concentration (HbR). HbR and CBV changes are also used for human brain mapping in blood oxygenation level-dependent (BOLD) fMRI, a technique that was developed soon after optical imaging (10–12).

Although CBF, CBV, and HbR changes have been used to obtain functional maps of neuronal electrical activity, little is known about the dynamics of neurovascular coupling, the underlying mechanisms, and the cortical metabolic processes affecting these changes. Controversies have emerged because of difficulties in interpreting the signals measured by the above imaging techniques, in characterizing and quantifying the metabolic processes, and in selectively measuring hemodynamic changes (e.g., HbR without CBV) from each vascular compartment.

By using imaging spectroscopy, which allows selective measurement of both HbR and HbO_2, we have recently demonstrated (13) that Hb-oxygenation changes in response to neuronal activation are biphasic; an early (<3 s), localized increase in HbR (often referred to as the "initial dip") is followed by a delayed decrease in HbR and a concomitant increase in HbO_2. Furthermore, the HBO_2 increase is spatially less well registered with the activated cortical columns relative to the early HbR increase [figure 3 in Malonek and Grinvald (13)]. A possible implication of these findings is that the early deoxygenation may provide a higher spatial resolution for fMRI neuroimaging than the conventionally used delayed hyperoxygenation response. Furthermore, the early Hb-deoxygenation-based methods may provide higher spatial resolution than CBF-based methods.

The time course of the HbR change and the existence of the "initial dip" has been confirmed only recently by high magnetic field fMRI (14), raising the question of what, precisely, is being measured by most other BOLD fMRI studies. It is therefore necessary to clarify the temporal relationship between cerebral blood flow, volume, and oxygenation during functional activation. This has never been determined experimentally. In this study we therefore investigate this relationship and specifically address the following questions. Is the early activation-induced increase in HbR caused by an increase in cerebral metabolic rate of oxygenation ($CMRO_2$) without matching CBF response? Does an increase in resting CBF affect the activation-induced changes? The answers to these questions are not only relevant to functional neuroimaging in humans, but may also further our understanding of the basic mechanisms of neurovascular coupling.

The publication costs of this article were defrayed in part by page charge payment. This article must therefore be hereby marked "*advertisement*" in accordance with 18 U.S.C. §1734 solely to indicate this fact.

Abbreviations: PET, positron-emission tomography; fMRI, functional MRI; CBF, cerebral blood flow; CBV, cerebral blood volume; BOLD, blood oxygenation level dependent; LDF, laser Doppler flowmetry.

†To whom reprint requests should be addressed.

MATERIALS AND METHODS

This study is based on experiments performed in six cats. In two of the cats conventional optical imaging of intrinsic signals was performed in combination with laser Doppler flowmetry (LDF). In the other four cats, imaging spectroscopy (optical imaging with high spectral resolution) was performed concurrently with the LDF. The procedures for conventional optical imaging, imaging spectroscopy, and LDF are outlined below in chronological order during a typical experiment. Additional details may be found in previous publications for optical imaging (7, 8, 15), imaging spectroscopy (13), and LDF (16–18).

Animals. Anesthesia was induced by ketamine hydrochloride (10–20 mg/kg i.m.) followed by sodium pentothal (20 mg/kg per h, i.v.). A headset was implanted over the anterior part of the skull to allow attachment of the head with minimal trauma. Animals were then placed in the stereotactic apparatus by using the headset attachment. A round opening was cut in the skull overlying area 17 and 18 and the dura was carefully resected. A cranial window chamber filled with inert solution and sealed with a transparent disk was placed over the opening and anchored to the skull with screws and dental cement. The animals were paralyzed (succinylcholine hydrochloride, 20 mg/kg/h) and artificially respirated. They received anesthetics and paralytics throughout the experiment and the heart rate, EEG, end-tidal CO_2, and temperature were constantly monitored. Blood pressure was monitored during the last four experiments. The corneas were fitted with zero power contact lenses and atropine (1%) was administered to paralyze accommodation. The eyes were focused on a tangent screen at a distance of 57 cm by using appropriate lenses, as determined by retinoscopy.

Visual Stimulation. The primary stimuli that were used in this study were vertical and horizontal moving gratings (high contrast, 0.3 cycles/degree; duty cycle = 0.2, 18°/sec) and a blank screen. The stimulation was binocular all along, with both eyes converged and focused on a stimulus screen [distance = 57 cm, extent = 40° (h) × 30°(v) contralateral to the imaged hemisphere]. During each experiment, the different stimuli were presented for 2–10 sec followed by a blank screen for an additional 15–30 sec. Each stimulus was presented 24–64 times during each experiment, and the order of appearance was randomized. Each curve in the figures is the calculated average of these repetitions.

Optical Imaging. Procedures were similar to those described elsewhere (7, 8, 15). In brief, intrinsic optical signals evoked by the visual stimuli were recorded by using an enhanced video system (Imager 2001, Optical Imaging, Germantown, MD) attached to a macroscope (19). The exposed cortex was illuminated with orange or green light (570 or 605 nm), and the reflected light was collected by the camera through the glass window of the chamber. Images were acquired at 2 Hz and stored to disk.

Imaging Spectroscopy. Procedures were similar to those described in an earlier publication (ref. 13; for *in vivo* single location spectral measurements, see ref. 20). In brief, the cortex was examined by using a two-tandem-lens macroscope that formed two image planes. The image in the first image plane was masked by an opaque disk with a transparent slit that was positioned in a selected image location, which showed a marked segregation of orientation columns. A dispersing grating, whose grooves were parallel to that slit, was positioned between the objective and the imaging lens of the second macroscope. Thus, the recorded image (second image plane) represented multiple displaced images of the slit, the degree of displacement varying with wavelength. We refer to these images as spatiospectral images. The spatial resolution of our spectroscope was better than 200 μm in the relevant spectral range, and the spectral resolution was better than 4 nm.

Laser Doppler Flowmetry. A main goal of this study was to temporally and spatially correlate activity-dependent Hb-oxygenation changes with changes in regional cerebral blood flow (rCBF).

LDF (21) is based on the recording of the Doppler shifts that occur when mobile red blood cells scatter monochromatic light. Principles and technical details have been described elsewhere in great detail (22, 23). A number of studies have validated the use of LDF to measure quantitatively changes in rCBF (16–18). However, absolute CBF values (blood perfusion per tissue volume) measured with LDF do not correlate well with quantitative CBF as measured with [^{14}C]iodoantipyrine autoradiography and hence were not used in this study. The sample volume of LDF is affected mainly by probe geometry, wavelength, and distance of the probe from the tissue. With the equipment and setup used here, the sample volume was estimated to be approximately 1 mm^3.

We used a Periflux 4001 (Perimed, Stockholm; wavelength of 780 nm) laser Doppler flowmeter to which a needle probe (Perimed PF 403; outer diameter, 450 μm; fiber separation, 250 μm) was attached. The probe was advanced at an angle of 45° through a tightly sealed hole in the cover glass of the cranial window and reached a position $<$1 mm from the brain surface. By using the imaging spectroscope, the positioning of the probe and thus the focus of the sample volume were checked and adjusted by visual monitoring of the near-infrared spot projected on the brain surface by the laser beam (Fig. 1*A*). Thus, a complete spatial registration of cortical area monitored by imaging spectroscopy and LDF was attained. The time constant of the LDF was set to 0.03 seconds, and the LDF readings were digitized at 100 Hz, transferred to computer memory, and saved to disk. We also verified that the delay of the LDF response to an instantaneous flow change was shorter than 0.1 sec.

Experimental Procedure. The experiment was carried out as follows. First, optical imaging of orientation maps was performed through the double-tandem-lens system. Images of the exposed cortical surface (epi-illumination with 100-W halogen lamp, λ = 605 nm) were collected, and functional orientation maps were obtained by computing the difference between images obtained during visual stimulation by moving gratings of orthogonal orientations. Only after observing segregated orientation columns in the calculated differential functional maps did we continue with the spectroscopic and LDF measurements. The optical imaging system was modified into an imaging spectroscope, and a broad-spectrum light source (500–700 nm) was used to illuminate the cortical surface [details in Malonek and Grinvald (13)]. The data collection procedure remained unchanged: spatiospectral images were accumulated by the video camera and digitized at a video rate of 25 Hz. These frames were averaged on-line, lowering the time resolution to 2 Hz for the off-line analysis. The LDF probe was inserted through the rubber gasket and targeted to the same cortical area.

Data acquisition of the LDF, optical imaging, and imaging spectroscopy were synchronized to the respirator and heart beat as described elsewhere (7, 8, 15).

Spectral Analysis. From the intensity variations in the image it was possible to obtain the reflection spectrum of each image point along the slit. The intensity profile of a given horizontal line represented the reflection spectrum of a given location in the imaged specimen. Horizontal lines at right angles to these had an intensity profile that represented the variation along the selected slit-like image of cortex at a given wavelength. The comparison of reflection spectra taken from different locations was readily performed by comparing the intensity profiles from the appropriate locations within a single image. The spatiospectral images were analyzed by comparing the images acquired during visual stimulation with those acquired during

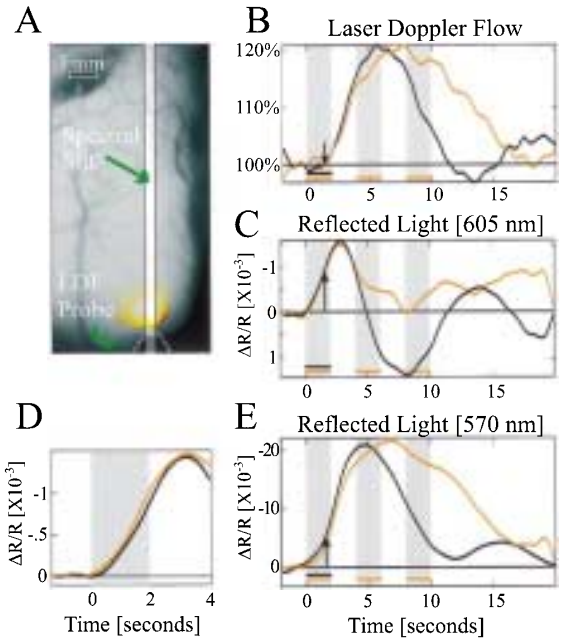

FIG. 1. Simultaneous measurement of cortical reflection and CBF. (*A*) An image of the cortical surface, the location of slit used for imaging spectroscopy, the tip of LDF probe, and the reflection of its beam from the cortex. The yellow spot marks the cortical region that was illuminated by the LDFs laser during the measurements. (*B*, *C*, and *E*) Cortical response to visual stimulation. Black curves represent response to short stimulus (2 sec), and red curves represent its response to long stimulus (10 sec, composed of 2 on, 2 off, 2 on, 2 off, 2 on). Each curve is the average response to 24 stimulation periods during a single experiment. (*B*) LDF response. Its onset (arrow) lags after stimulus onset by ≈1.5 sec. (*C*) Cortical reflection change: 605-nm illumination. The response is biphasic, and its onset leads the LDF response by ≈1 sec. Long stimulus duration attenuates the second phase, which almost vanishes. Notice that increased reflection is downward. (*D*) The vascular response ("initial dip") at different flow levels and at different times after the stimulus onset. We compare the early response to the short stimulus (black curve in *C*), when CBF was at equilibrium, with that obtained when CBF was elevated and a second delayed stimulus followed, by subtracting the short stimulus curve from the long stimulus curve (red curve in *C*). In *D*, when this difference, i.e., the net response to the second stimulus, shown in red, is shifted in time and superimposed on the response to the first stimulus (black line), the two curves are nearly identical. The second stimulus was given when CBF increased by ≈15%. (*E*) Cortical reflection change: 570-nm illumination. Similar to reflection changes at 605-nm illumination, the response onset leads the LDF response by 1 sec. The response is maintained throughout stimulus duration, for both short and long durations.

blank screen. Changes in the reflected light were modeled by the following formula:

$$\Delta R_\lambda(t) = K_1(t)\cdot\varepsilon_{HbO_2} + K_2(t)\cdot\varepsilon_{HbR} + LS(t) + E(t),$$

where $K_1(t)$ is a relative parameter related to the product of HbO_2 and the optical pathlength, and $K_2(t)$ is similarly related to HbR. $LS(t)$ (light scattering) is related to changes of the tissue's refractive index, and $E(t)$ is the residual error term. By using a linear least squares fit routine, the above equation was fit to the intensity profile along each line in each spatiospectral image, for a spectral range of 530–650 nm. The fit was good and the root mean square of error (difference between the measurements and the modeled curve) was less than 5% in most experiments. Other models for the light-scattering contribution neither improved the goodness of fit nor changed the main results outlined here for HbR and HbO_2.

RESULTS

Stimulus-Evoked CBF and Optical Reflectance Responses. To compare CBF changes to optical reflectance changes we simultaneously measured the time course of the CBF and the activity-dependent reflected signals at either one of two wavelengths (605 and 570 nm) in response to visual stimulation. A short, 2-sec visual stimulation with moving-oriented gratings induced both blood flow (Fig. 1*B*) and reflectance changes (Fig. 1 *C* and *E*), which persisted for more than 10 sec (black curves). The cortical reflectance changes at 605 ± 5 nm illumination (Fig. 1*C*) had a stereotypical biphasic shape; an initial decrease in reflectance ($\Delta R/R = -1.5 \times 10^{-3}$) followed by an increase in cortical reflectance ($\Delta R/R = 1.5 \times 10^{-3}$; a decreased reflectance, i.e., cortical darkening, is assigned negative numbers but plotted upward). The observed reflectance changes result from changes in both light absorption and light scattering in the tissue. The dynamics of CBF changes were strikingly different (Fig. 1*B*): the onset (arrows in Fig. 1 *B*, *C*, and *E*) was delayed by more than 1 sec after the reflectance signal onset, and its shape was monophasic rather than biphasic. The CBF response reached its maximal change of ≈20% approximately 4 sec after stimulus termination and returned to baseline within an additional 8 sec. The dynamics of CBF changes observed here (Fig. 1*B*) were in good agreement with previous LDF studies (24).

It already has been shown that changes in cortical reflectance at 605 nm can be used to approximate HbR changes, whereas at 570 nm (Hb-isosbestic point), blood volume changes are emphasized (7, 13). As in previous observations, cortical reflection changes at 570 nm (Fig. 1*E*) were markedly different from those at 605 nm (Fig. 1*C*). However, the blood volume changes (major component of curve in Fig. 1*E*) and the CBF-LDF curves (Fig. 1*B*) display an apparent similarity, indicating that flow and volume dynamics are more similar than flow and HbR changes. The major exception is at short latencies, where, as at 605 nm, the onset of the reflected light response at 570 nm precedes the onset of the blood flow response (indicated by the arrow) by more than a second. This suggests that the blood flow onset is delayed relative to the onset of both HbR and blood volume increases.

To study the responses to longer stimulation we used a train of three short stimuli (interlaced periods of 2 sec of grating stimulus, 2 sec of blank stimulus). CBF and cortical reflection (605-nm illumination) were altered differently, whereas CBF continued to increase and remained elevated throughout the stimulation; by contrast, the second phase of cortical reflectance at 605 nm was reduced (Fig. 1 *B* and *C*, red curves). Again, the blood volume change estimated by the 570-nm measurement was similar to the CBF response, except in the period immediately after the onsets of both responses.

Dynamics of Stimulus-Evoked CBF, Blood Oxygenation, and Total Hemoglobin Responses. Reflectance measurements at a single wavelength, as the ones described above, cannot be used to estimate HBO_2 and are only a first approximation for HbR and blood volume changes. To quantify various biochemical and physiological manifestations of the cortical response to activation we employed imaging spectroscopy. By using this technique, we measured cortical reflectance changes at multiple wavelengths and multiple locations simultaneously as a function of time. From these spectra we extracted the time course of the changes in the individual components, HbR, HBO_2, and Hbt (see *Methods*) and compared them with the simultaneously measured CBF response (Fig. 2). We found a striking similarity between the HbO_2 and CBF responses (Fig. 2); the CBF and HBO_2 curves are almost identical in their

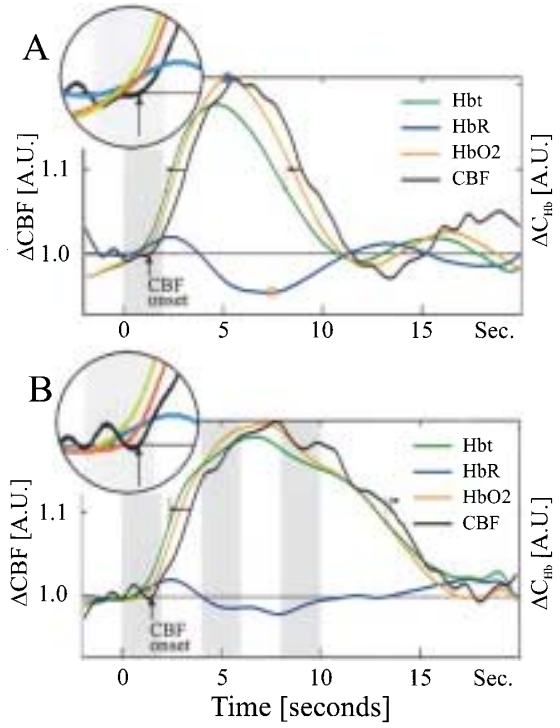

FIG. 2. Dynamics of various vascular responses. Total hemoglobin concentration (Hbt, green line) leads CBF response (black line) throughout the response cycle for both the short stimulus (*A*) and the repeated stimuli (*B*). Each curve is the average response to 24 stimulation periods during a single experiment. Horizontal arrows mark the temporal difference between the curves when they had reached 50% of their maximal amplitude (marked by thin, vertical lines) during the uprising phase and during the decay to baseline. HbR curve appears to lead all other components, and it reaches its peak before all other curves. Notice the delays of both the CBF (marked by arrow) and the HbO_2 onsets after the stimulus onsets. At onset, Hbt change is entirely composed of HbR elevation, whereas at the later phase it is predominantly HbO_2. Because of fluctuations of HbO_2 (and thus Hbt) before stimulation, its onset is determined as time when its rate of change increased. Asterisks mark the maximum of HbO_2 and the minimum of HbR.

onset, rise time, and decay to baseline for both short- and long-stimulus durations.

The dynamics of the HbR response was drastically different from both CBF and HbO_2 responses (Fig. 2). Its time course (blue curve) had a stereotypical biphasic shape as compared with the monophasic shapes of both the CBF and the HbO_2 curves. Furthermore, the onset of the HbR increase preceded the onset of CBF increase by more than a second (e.g., Fig. 2*B Inset*) whereas its time to peak was shorter by more than 3 sec. The delayed onset of CBF response (>1.3 sec) was observed repeatedly in all the experiments during this study ($n = 6$). This is consistent with the interpretation that the HbR time course results from two competing mechanisms; the early HbR increase is a result of an increase in $CMRO_2$, whereas the later increase in CBF causes the reduction in HbR and the subsequent undershoot. Note that the time course of HbR (Fig. 2) resembles that of the cortical reflection change at 605 nm (Fig. 1*C*, black), which has been used as an approximation for this chromophore.

To shed light on the mechanisms that underlie these events in microcirculation, we focused on the first 2 sec of the response (Fig. 2 *Insets*). During the initial first second of functional activation, the only observable change was indeed an increase in deoxyhemoglobin (i.e., increase in HbR), and no change in CBF was observed during this phase (Fig. 2). At 1 sec after stimulation, the elevated HbR has reached ≈30% of its peak value whereas the change in CBF (if at all occurred) was less than 4% of its peak value (Figs. 1*B* and 2*A Inset*). These observations, together with the lack of a concomitant decrease in HbO_2, imply that during this period an increase in total hemoglobin concentration ($\Delta Hbt = \Delta HbR + \Delta HbO_2$) occurred (Fig. 2, green lines). Thus, we suggest that the activity-induced rise in $CMRO_2$ leads to an increased extraction of O_2 and a simultaneous but independent increase in the total hemoglobin concentration. This is at a time when CBF has not yet started to increase in response to the stimulus. Further examination of the different curves showed that the rate of change in HbR started to decrease at the onset of both CBF and HbO_2 changes (see also Fig. 3). One likely interpretation is that arteriolar vasodilatation causes an outwash of the increased HbR produced by the increased oxygen consumption ($CMRO_2$). During the phase of increased cerebral blood flow leading to blood hyperoxygenation, HbR is no longer a measure of the increased oxygen consumption exclusively, but rather reflects the net effect of $CMRO_2$-induced blood deoxygenation together with the flow-induced blood hyperoxygenation.

We further observed that the stimuli with short duration elicited concentration changes that continued for a long time after their termination. HbO_2, Hbt, and CBF continued to increase and reached a maximum only after 5 sec, and at the same time HbR decreased (Fig. 2*A*). A delay between the time point at which CBF reached its maximum and the time point when HbR reached its minimum was observed (asterisks in Fig. 2*A*). This is in contrast with the inverse relationship observed after the onset of stimulation, when HbR leads the CBF response by more than a second. This delay is compatible with the assumption that $CMRO_2$ starts to diminish before CBF starts to decline.

The temporal relations between Hbt and CBF can shed light on the underlying vascular regulatory processes (Fig. 2). The changes in Hbt lead the changes in CBF by more than a second throughout the response. The initial increase in Hbt was composed primarily of an increase in HbR, and thus early in the response, HbR changes lead the changes in CBF. At a later phase, Hbt changes were composed primarily of HbO_2 changes, which lead the changes in CBF and HbR.

To emphasize the temporal relationships of CBF, HbR, and Hbt we display the same results in the form of phase plots: ΔHbR vs. ΔCBF (Fig. 3*A*) and ΔHbt vs. ΔCBF (Fig. 3*B*). In these plots, a simultaneous covariation of the parameters appears as a straight, tilted line, whereas a delayed covariation appears as a curved line or a tilted ellipsoid.

After the initial increase of HbR and the delayed onset of a CBF change (arrow in Fig. 3*A*), the phase plot transforms into a curved line, indicating the inverse but delayed variation of both ΔHbR and ΔCBF. At the final phase of the response (its onset marked by an asterisk), these parameters co-vary along a straight line, reflecting an inverse relation without delay. Evidently, the increase in flow results in a decreased HbR, whereas a CBF decrease causes an elevation in HbR. These temporal relationships between ΔCBF and ΔHbR are consistent with two different physiological states: during the first period, $CMRO_2$ (and thus the HbR level) was elevated by the stimulation and the delayed blood flow caused a delayed reduction in HbR. The delayed and inverse relationship between ΔCBF and ΔHbR was caused by the decrease in $CMRO_2$, which slowly returned to equilibrium over this period. During the second period, when $CMRO_2$ was already at equilibrium, any change in ΔCBF was reflected directly as an inverse change in ΔHbR. Similarly, in Fig. 3*B*, we observed that blood volume changes (ΔCBV) lead the ΔCBF changes (ar-

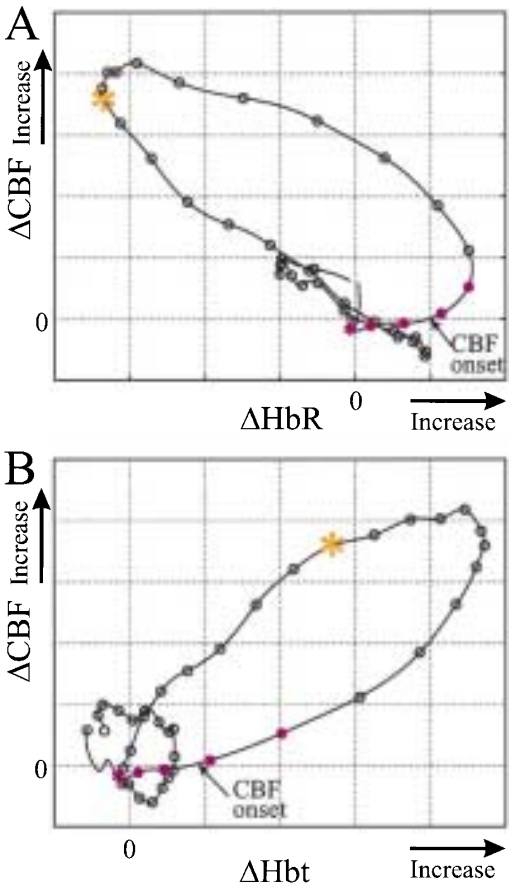

FIG. 3. Correlated dynamics of CBF to HbR and to Hbt for short stimulus. Phase plots show the dependence of CBF changes on HbR and Hbt after 2 sec of stimulation. Along the curves, intervals between the circles represent 0.5 sec, and the first four segments (five circles) are during stimulation. An asterisk marks the stimulus onset, and an arrow marks the onset of CBF, when an observable change in its rate of change is detected. (*A*) After stimulation onset (pink asterisk), HbR increases, whereas no observable change in CBF is seen for more than a second. As CBF starts to increase (arrow), the rate of change of HbR starts to decrease and becomes negative 1 sec later. At the last phase of the response (red asterisk), an inverse relation between the parameters is seen; an increase in CBF is accompanied by a decrease in HbR and *vice versa*. (*B*) An exponential dependence of CBF on Hbt is seen during the first 4.5 sec after stimulus onset. Throughout the response cycle, changes in Hbt lead changes in CBF by about 1–2 sec.

rows in Fig. 2*A* and an ellipsoid shape in Fig. 3*B*) throughout the response period.

The temporal relations between Hbt and CBF changes are not consistent with the hypothesis that blood flow changes induce blood volume changes, but rather the opposite! From these two phase plots one can hypothesize that the variations in Hbt induce blood flow changes throughout the response cycle. Sensory stimulation increases $CMRO_2$ (and thus HbR) and induces a perturbation in Hbt by local dilation of the vessels, which lasts for many seconds. The elevation of blood volume (and Hbt) induces a delayed blood flow change, which in turn induces a decrease in HbR. It is not possible to observe the changes in $CMRO_2$ selectively by monitoring HbR, because both $CMRO_2$ and flow induce changes in HbR. However, we may deduce the dynamics of $CMRO_2$ from the temporal relationship between ΔHbR and ΔCBF. While the $CMRO_2$ was slowly returning to baseline, HbR was delayed relative to CBF. At a later period (5–18 sec after stimulus termination; the beginning of this period is marked by the asterisk in Fig. 3*A*), any change in CBF was mirrored directly as an inverse change in HbR: an increase in flow causes a reduction in HbR whereas a decrease in flow causes an elevation in HbR. These results are consistent with constant $CMRO_2$ and functional recruitment of capillaries (see *Discussion*).

DISCUSSION

Correlation Between Imaging Spectroscopy and LDF. In the present study we used optical techniques to differentiate several manifestations of the vascular events associated with sensory activation of cortex. By using the spectrum of reflected light from activated cortex we were able to extract the alterations in blood oxygenation and total hemoglobin concentration. A simple linear model was used to estimate variations in HbR, HbO_2, and light-scattering components from the spectral changes. We were concerned that our model might not be sufficiently rigorous and that this might compromise the analytical results and their interpretation. In a previous report (13) we stated that the results were not sensitive to more complicated models of light scattering. The current study with simultaneous LDF measurements lends additional support to our previous conclusions, derived from imaging spectroscopy alone. In particular, we can consolidate our description of the sequence of vascular events following sensory activation. (*i*) As soon as blood flow, as measured by the LDF, increased, the HbO_2, as measured by imaging spectroscopy, also increased (Fig. 2). (*ii*) The rate of change in HbR started to decrease as soon as a blood flow increase was detected by the LDF measurement (Fig. 2*A Inset*). Thus, these two very independent measurements (e.g., imaging spectroscopy and LDF) provide mutually consistent results that strengthen the reliability of both methodologies.

Implications for fMRI. Functional activation of the human brain based on activity-dependent CBF responses can be imaged with PET or flow-sensitive MRI. However, optical imaging has shown that functional maps exclusively based on a this secondary vascular response may offer a lower spatial resolution than the initial HbR increase that is localized to the sites of elevated neuronal firing. The delayed HBO_2 increase occurred to an almost equal degree in both activated and nearby nonactivated cortical columns (compare figure 3 B and C in ref. 13). Because the delayed HBO_2 component, which originates from the blood flow increase, is poorly localized, its associated HbR decrease must also be poorly localized. We found that increasing the stimulus duration reduced the signal to noise in maps of functional cortical domains.

Most fMRI studies have been unable to detect the "initial dip" in blood oxygenation observed with optical imaging. However, a few recent studies indeed have confirmed that such an initial increase in HbR can be observed by using high-field-strength fMRI (14, 25). Consequently, the question of whether BOLD-fMRI can detect the very early increase in HbR currently is subject to controversy. The data presented here suggest that the early blood deoxygenation occurs concurrently with an increase in total hemoglobin concentration (Fig. 2*A*). It is possible that the increase in total hemoglobin concentration is accompanied by blood volume changes and by functional capillary recruitment, whose exact effects on the BOLD signals is not yet known. Thus, there is currently a disagreement between the dynamics of HbR, as measured by imaging spectroscopy and PO_2 as previously measured by an ion-selective microelectrode (26) on the one hand, and the BOLD signal, as measured by fMRI on the other. This question warrants extensive exploration.

Vascular Regulation at the Capillary Level. The present data and previous studies (8, 13) demonstrate that the metabolic consequence of functional activation (i.e., increased HbR because of increased O_2 demand) reaches the microvasculature less than 500 msec after stimulation onset. Interestingly, this increase in HbR cannot entirely be accounted for by deoxygenation of HbO_2, because we did not find the expected HbO_2 decrease. Rather, we observed that Hbt levels also increased at this early phase of the response, before the CBF change in the activated tissue. This apparently surprising fast increase in total hemoglobin concentration forced us to search for a suitable physiological mechanism that can explain these data. One possibility is that this early Hbt increase indeed reflects blood volume increase at the capillary bed, which currently is a controversial notion (27, 28). Regulation at the capillary level is also compatible with our ability to visualize individual functional columns whose size is often less than 200 μm, a size that would be too small to visualize if the regulation of blood volume were to occur in any of the other vascular compartments alone. Although capillaries per definition do not contain smooth muscle cells, they are surrounded by pericytes (29). This latter cell type is contractile and reacts to a number of stimuli implicated in cerebrovascular coupling (nitric oxide, drop in pH, ATP, adenosine) with dilatation. For this reason, pericytes have been suggested as an active element involved in capillary blood flow regulation (29).

"Functional Recruitment" of Capillaries. Functional recruitment (30) of capillaries is the transition of low-flow capillaries to high-flow capillaries (28). One might envision a very early phase of activation when local capillary corpuscular blood volume increases, but at a time when arterioles have not yet dilated and the blood flow has not yet increased. Although not very intuitive at first sight, this type of delayed relationship between blood volume and blood flow is possible if the outflow from the capillary compartment in the activated cortical columns is temporarily lower than the inflow to this capillary compartment. This type of scenario might arise if the capacitance of the capillaries were to increase and their resistance were to decrease following the electrical activity. In other words, because of the increased capacitance of this vascular compartment, where resistance is comparatively low, the capillary bed might act as "sink" for red blood cells, allowing the outflow from the compartment to drop, before the occurrence of upstream arteriolar dilatation that would cause an increased inflow. Subsequently, when the arteriolar segment has dilated, the increased inflow causes a flow increase in the entire capillary compartment, HbO_2 increases, and HbR decreases. Because in most cortical areas the arterioles do not feed selectively individual functional domains, this flow increase is less localized to the site of increased electrical activity.

The early functional capillary recruitment is consistent with our previous report (8). After loading the microcirculation with a fluorescent dextran, an increase in blood volume was detected in response to visual stimulation. The ability to obtain high-resolution functional maps upon selectively imaging these blood volume changes indicated that a significant portion of this change must have taken place in capillaries rather than another vascular compartment.

We thank Dr. Louis Sokoloff for his constructive comments. We also thank D. Ettner, N. Dekel, and C. Weijbergen for their technical support. This work was supported by grants from Ms. Margaret Enoch, the Minerva foundation, and the Wolfson Foundation to A.G.

1. Roy, C. & Sherrington, C. (1890) *J. Physiol.* **11,** 85–108.
2. Ketty, S. S. & Schmidt, C. F. (1945) *Am. J. Physiol.* **143,** 53–66.
3. Sokoloff, L., Reivich, M., Kennedy, C., Des Rosiers, M. H., Patlak, C. S., Pettigrew, K. D., Sakurada, O. & Shinohara, M. (1977) *J. Neurochem.* **28,** 897–916.
4. Chance, B., Cohen, P., Jobsis, F. & Schoener, B. (1962) *Science* **137,** 499–502.
5. Fox, P. & Raichle, M. (1985) *Ann. Neurol.* **17,** 303–305.
6. Raichle, M. (1994) *Sci. Am.* **270,** 58–64.
7. Grinvald, A., Lieke, E., Frostig, R. D., Gilbert, C. D. & Wiesel, T. N. (1986) *Nature (London)* **324,** 361–364.
8. Frostig, R. D., Lieke, E. E., Ts'o, D. Y. & Grinvald, A. (1990) *Proc. Natl. Acad. Sci. USA* **87,** 6082–6086.
9. Belliveau, J., Kennedy, D., McKinstry, R., Buchbinder, B., Weisskopf, R., *et al.* (1991) *Science* **254,** 716–719.
10. Ogawa, S., Tank, D., Menon, R., Ellerman, J., Kim, S., *et al.* (1992) *Proc. Natl. Acad. Sci. USA* **89,** 5951–5955.
11. Kwong, K., Belliveau, J., Chesler, D., Goldberg, I., Weisskoff, R., Poncelet, B., Kennedy, D., Hoppel, B., Cohen, M., Turner, R., Cheng, H., Brady, T. & Rosen, B. (1992) *Proc. Natl. Acad. Sci. USA* **89,** 5675–5679.
12. Turner, R., Jezzard, P., Wen, H., Kwong, K., Le Bihan, D., *et al.* (1993) *Magn. Reson. Med.* **277,** 279.
13. Malonek, D. & Grinvald, A. (1996) *Science* **272,** 551–554.
14. Menon, R. S., Ogawa, S., Hu, X., Strupp, J. P., Anderson, P. & Ugurbil, K. (1995) *Magn. Reson. Med.* **33,** 453–459.
15. Ts'o, D. Y., Frostig, R. D., Lieke, E. E. & Grinvald, A. (1990) *Science* **249,** 417–420.
16. Dirnagl, U., Kaplan, B., Jacewicz, M. & Pulsinelli, W. (1989) *J. Cereb. Blood Flow Metab.* **9,** 589–596.
17. Fabricius, M. & Lauritzen, M. (1996) *J. Cereb. Blood Flow Metab.* **16,** 156–161.
18. Haberl, R. L., Heizer, M. L., Marmarou, A. & Ellis, E. F. (1989) *Am. J. Physiol.* **256,** H1247–H1254.
19. Ratzlaff, E. H. & Grinvald, A. (1991) *J. Neurosci. Methods* **36,** 127–137.
20. LaManna, J. C., Sick, T. J., Pikarsky, S. M. & Rosenthal, S. M. (1987) *Am. J. Physiol.* **253,** C477–C483.
21. Stern, M. D. (1975) *Nature (London)* **254,** 56–58.
22. Bonner, R. & Nossal, R. (1981) *Appl. Opt.* **20,** 2097–2107.
23. Shepherd, A. P., Riedel, G. L., Kiel, J. W., Haumschild, D. J. & Maxwell, L. C. (1987) *Am. J. Physiol.* **252,** G832–G839.
24. Lindauer, U., Villringer, A. & Dirnagl, U. (1993) *Am. J. Physiol.* **264,** H1223–H1228.
25. Hu, X., Le, T. H. & Ugurbil, K. (1997) *Magn. Reson. Med.* **37,** 877–884.
26. Silver, I. (1978) in *Cerebral Vascular Smooth Muscle and Its Control*, eds. Elliott, K. & O'Connor, M. (Elsevier, New York), pp. 49–61.
27. Weiss, H. R. (1988) *Microvasc. Res.* **36,** 172–180.
28. Kuschinsky, W. & Paulson, O. B. (1992) *Cerebrovasc. Brain Metab. Rev.* **4,** 261–286.
29. Tilton, R. G. (1991) *J. Electron Microsc. Technol.* **19,** 327–344.
30. Villringer, A. & Dirnagl, U. (1995) *Cerebrovasc. Brain Metab. Rev.* **7,** 240–276.

Measurement of glucose uptake and intracellular calcium concentration in single, living pancreatic β-cells*

Katsuya Yamada‡, Masanori Nakata‡, Naoki Horimoto‡, Mikako Saito§,
Hideaki Matsuoka§, and Nobuya Inagaki‡

‡ Department of Physiology, Akita University School of Medicine, 1-1-1,
Hondo, Akita 010-8543, Japan
§Department of Biotechnology, Tokyo University of Agriculture
and Technology, 2-24-16, Nakamachi, Koganei, Tokyo 184-8588, Japan.

和文要約

哺乳動物細胞内へのグルコース輸送は、これまで主に放射性標識グルコースにより解析されてきた為、単一細胞レベルでのリアルタイムの観察が困難であった。今回申請者らは、新規蛍光標識2-デオキシグルコース（2-NBDG）が、哺乳動物細胞にグルコーストランスポーターを介して特異的に取り込まれかどうかを検討し、更に単一膵島細胞を対象としてグルコース取り込みとその他の細胞機能をリアルタイムに評価することを目的として研究を行なった。実験の結果、2-NBDGは哺乳動物細胞内にグルコーストランスポーターを介して特異的に取り込まれること、およびその取り込みはD-グルコースに類似していることが明らかとなった。また膵β細胞はα細胞に比較してグルコース取り込みが大きく、またそのインスリン分泌に伴う$[Ca^{2+}]_i$上昇には、グルコース取り込みと同時にグルコースの細胞内代謝が重要であることが示唆された。以上により、新規蛍光標識2-デオキシグルコース（2-NBDG）を用いる全くグルコース輸送研究手法を確立する事ができ、本法を脳細胞に適用することで今後のグルコース研究に新たな展開が期待される。

SUMMARY

There has been no method previously to measure both glucose transport and its effect on the various intracellular functions in single, living mammalian cells. A fluorescent derivative of D-glucose, 2-[*N*-(7-nitrobenz-2-oxa-1,3-diazol-4-yl)amino]-2-deoxy-D-glucose (2-NBDG) that we have developed has made such measurements possible. COS-1 cells that overexpress the human glucose transporter GLUT2 show significantly greater 2-NBDG uptake than mock-transfected cells. Using GLUT2-abundant mouse insulin-secreting clonal MIN6 cells, we found that 2-NBDG was incorporated into the cells in a time- and concentration-dependent manner. The 2-NBDG uptake was inhibited by high concentrations of D-glucose in a dose-dependent manner, and also was almost completely inhibited by 10 μM cytochalasin B. We then measured both glucose uptake and the intracellular calcium concentration ($[Ca^{2+}]_i$) in single, living pancreatic islet cells. 2-NBDG and fura-2 were used as the tracer of glucose and indicator of intracellular calcium, respectively. All of the cells that showed an increase in $[Ca^{2+}]_i$ in response to a high concentration of glucose (16.8 mM) rapidly incorporated significant 2-NBDG. Immunocytochemical examination confirmed these cells to be insulin-positive β-cells. All of the cells that showed no significant, rapid 2-

NBDG uptake lacked such glucose responsiveness of $[Ca^{2+}]_i$, indicating that these cells were non-β-cells such as glucagon-positive α-cells**.** These results show the uptake of glucose causing a concomitant increase of $[Ca^{2+}]_i$ in β-cells. Because 2-NBDG is incorporated into mammalian cells through glucose transporters, it should be useful for the measurement of glucose uptake together with concomitant intracellular activities in many types of single, living mammalian cells.

INTRODUCTION

Glucose transport activity in mammalian cells has been monitored by radiolabeled tracers such as [^{14}C] 2-deoxy-D-glucose (1), [^{18}F] fluoro-2-deoxy-D-glucose (2), and [^{14}C] or [^{3}H] 3-*O*-methyl-D-glucose (3, 4). Although these methods are quite effective in glucose utilization studies (5-7), they cannot measure glucose uptake in single, living cells.

We have recently developed a fluorescent D-glucose derivative, 2-[*N*-(7-nitrobenz-2-oxa-1,3-diazol-4-yl)amino]-2-deoxy-D-glucose (2-NBDG)[1] (8), that allows a more sensitive measurement of glucose uptake in real time in single, living cells. Another advantage of measuring glucose uptake by the 2-NBDG molecule is that it allows concomitant measurement of other cellular activities, such as the intracellular calcium concentration ($[Ca^{2+}]_i$), pH, or membrane potential by different methods. However, it has not been established that 2-NBDG is incorporated into mammalian cells, in which glucose is transported by facilitated diffusion through a family of glucose transporters GLUTs (9).

Among the several GLUTs identified to date, GLUT2 has high Km for glucose and is abundant in cells that sense glucose, such as pancreatic β-cells (9). It is thought that when the blood glucose level is elevated, glucose uptake into the pancreatic β-cells through GLUT2 is increased, and that this incorporated glucose is then metabolized within the cell. Among the various metabolic products, ATP is an essential molecule for insulin secretion (10); an increase in the intracellular ATP concentration in the β-cell closes the ATP-sensitive K^+ channel, leading to plasma membrane depolarization and influx of Ca^{2+} through the voltage-gated calcium channels. The subsequent rise in $[Ca^{2+}]_i$ triggers insulin secretion. However, the correlation between glucose uptake and changes in $[Ca^{2+}]_i$ in response to glucose stimulation has not been shown directly in single insulin-secreting β-cells.

To determine whether living, mammalian cells incorporate 2-NBDG through GLUT, we examined 2-NBDG uptake activity of cells in which GLUT2 is overexpressed or abundant, using fluorescence microscopy. We monitored glucose uptake activity and the $[Ca^{2+}]_i$ level in single, living pancreatic islet cells using 2-NBDG as a tracer of glucose and fura-2 as an intracellular calcium indicator. Our results suggest that 2-NBDG should be useful in analysis of the mechanisms underlying glucose uptake and concomitant cellular functions in mammalian cells.

EXPERIMENTAL PROCEDURES

Cell culture and transfection- Culture and transfection of COS-1 cells was carried out as described previously (11). Briefly, COS-1 cells were plated on 35 mm culture dishes at a density of 2 x 10^5 cells/dish 24 hours prior to transfection, and cultured in Dulbecco's modified Eagle's medium (450 mg/dl glucose) supplemented with 10 % fetal calf serum. Two micrograms of human GLUT2 expression vector (pCMVGLUT2) was transfected into COS-1 cells with LipofectAMINE and Opti-MEM I (Life Technologies, Inc., Gaithersburg, MD), according to the manufacturer's instructions. As control, COS-1 cells transfected with

vector (pCMV) alone were used. MIN6 cells were cultured in the same medium as COS-1 cells.

Preparation of rat islet cells- Islets of Langerhans were isolated from 8-12-week-old Harlan Sprague Dawley rats by collagenase digestion as described previously (12). Isolated islets were dissociated into single cells by incubation in Ca^{2+}-free Krebs Ringer bicarbonate buffer (KRB) containing 1 mM EGTA but no added Ca^{2+}. KRB was composed of (in mM): NaCl, 129; KCl, 4.7; KH_2PO_4, 1.2; $MgSO_4$, 1.2; $CaCl_2$, 2.0; $NaHCO_3$, 5.0; and HEPES, 10, pH 7.4, supplemented with 0.1 % bovine serum albumin. After centrifugation, the single cells were resuspended in Eagle's Minimum Essential Medium supplemented with 10% fetal bovine serum and 60 μg/ml kanamycin, plated on coverslips, and cultured up to 3 days at 37°C in a humidified atmosphere containing 5% CO_2.

Measurement of 2-NBDG uptake- The cells were mounted in a chamber and placed on the stage of an inverted microscope and superfused with KRB containing various concentrations of 2-NBDG at a flow rate of 0.3 ml/min (12). Delivery and removal of superfusate was by peristaltic or vacuum pump. Fluorescence of 2-NBDG was collected by a silicon intensified target camera at 520-560 -nm wavelength (excitation wavelength 465-495 nm). Images of 15-100 cells/each preparation were digitized in 8 bit, and integrated 16 or 64 times at video rate by an Argus-50 system (Hamamatsu Photonics, Hamamatsu, Japan). After background subtraction, fluorescence intensity was calculated as the difference in the average fluorescence of cells before and after application of 2-NBDG. Adequate neutral density filters were selected so that 2-NBDG fluorescence intensity was in the linear range of fluorescence versus concentration of 2-NBDG. In time and temperature dependence experiments, MIN6 cells (13) were superfused in D-glucose-free KRB for 15 min, and then the superfusate was changed to D-glucose-free KRB containing 600 μM 2-NBDG. After superfusion for the periods indicated at 25°C or 37°C, the cells were washed for 5 min, and the fluorescence images were collected. Concentration dependence experiments were carried out under the same condition except that the cells were superfused for 1 min at 37°C in D-glucose-free KRB containing the concentrations of 2-NBDG indicated. Similarly, the effect of D-glucose on 2-NBDG uptake was estimated by incubating the cells for 1 min at 37°C in KRB containing 600 μM 2-NBDG in the presence of the concentrations of D-glucose indicated. The effects of cytochalasin B and phloretin on 2-NBDG uptake were examined by superfusing the cells for 15 sec with 200 μM 2-NBDG in the presence of 5.6 mM D-glucose at 25°C; the experiments on overexpression of GLUTs in COS-1 cells were also performed under the same condition.

Measurement of $[Ca^{2+}]_i$ and 2-NBDG uptake- The islet cells were incubated with 1 μM fura-2/acetoxymethylester (14) for 30 min at 37°C in KRB containing 2.8 mM glucose. The cells were then mounted in the chamber and superfused with KRB containing a basal (2.8 mM) or elevated (16.8 mM) concentration of glucose at 37°C as described above. Fura-2 fluorescence was detected by a silicon intensified target camera every 5 or 10 sec at 500-520 -nm wavelength following excitation at 340-nm (F340) and 380-nm (F380) wavelengths, and the ratio image (F340/F380) was calculated by an Argus-50. After measurement of $[Ca^{2+}]_i$, 2-NBDG uptake into the same cells was estimated by superfusion at 37°C for 1 min in KRB containing 200 μM 2-NBDG and 2.8 mM D-glucose. In some experiments, the glucose-induced $[Ca^{2+}]_i$ response and 2-NBDG uptake were measured in the presence of 50 μM of 2,4-dinitrophenol (DNP). Because DNP has an effect of elevating basal $[Ca^{2+}]_i$ (15), high glucose was applied when this elevation was stabilized.

Immunocytochemistry- After measuring the fluorescence of 2-NBDG and $[Ca^{2+}]_i$, COS-1 cells or islet cells were fixed in 0.1 M sodium phosphate buffer containing 4 % paraformaldehyde, and pretreated with 1 % bovine serum albumin before incubation with anti-GLUT2, anti-insulin, or anti-glucagon antibody. For staining of GLUT2, the cells were incubated with rabbit anti-mouse GLUT2 antibody (1: 400) (Chemicon International Inc., Temecula, CA) for 1 hr at room temperature, followed by incubation with rhodamine-conjugated goat anti-rabbit IgG (1:500) (Cappel, West Chester, PA) for 20 min at room temperature. For staining β-cells, the cells were incubated with guinea pig anti-swine insulin antibody (1:100) (Dako Corp., Carpinteria, CA) at 4°C overnight, followed by incubation with rhodamine-conjugated goat anti-guinea pig IgG (1:500) (Chemicon International Inc., Temecula, CA) for 1 hr at room temperature. To stain α-cells, the cells were incubated with rabbit anti-porcine glucagon antibody (prediluted, Dako Corp., Carpinteria, CA) at 4°C overnight, followed by incubation with rhodamine-conjugated goat anti-rabbit IgG (1:100) (Cappel, West Chester, PA) at room temperature for 1 hr. Rhodamine fluorescence was examined by a silicon intensified target camera with a 590-nm longpass filter (excitation wavelength 510-560 nm).

RESULTS

2-NBDG uptake through mammalian glucose transporters - To determine whether 2-NBDG is transported through mammalian glucose transporters, we measured the uptake of 2-NBDG into cells overexpressing human GLUT2. The mammalian expression vector carrying GLUT2 cDNA (pCMVGLUT2) or vector alone (pCMV) was transfected into COS-1 cells, and 48 hours later the cells were loaded for 15 sec with the medium containing 200 μM 2-NBDG, followed by washout. Five minutes later, the fluorescence intensity of the cells was measured at 540-nm wavelength by fluorescence microscopy. COS-1 cells often showed granular autofluorescence in the cytosol before incubation in the presence of 2-NBDG (Fig. 1, B and G). After application of 2-NBDG, the fluorescence intensity of COS-1 cells transfected with GLUT2 expression vector was remarkably increased, and the cells can be more clearly discerned (Fig. 1, A-C). The net increase in fluorescence intensity of the cells is shown in Fig. 1D as a subtraction image; the fluorescence intensity before application of 2-NBDG was subtracted from that after its application. On the contrary, COS-1 cells transfected with the vector alone showed no remarkable difference in fluorescence before or after application of 2-NBDG (Fig. 1, F-I). These results were confirmed in eight separate experiments.

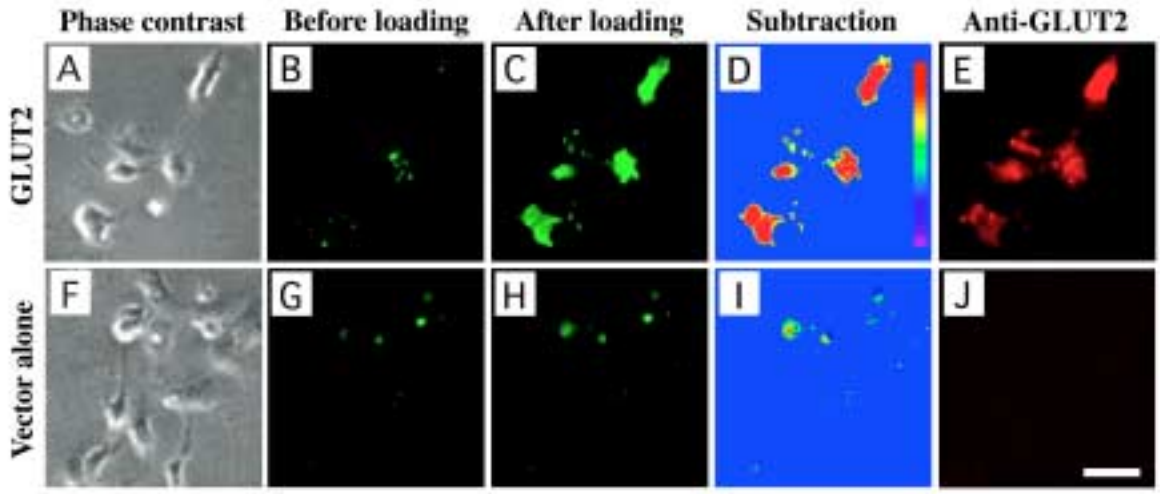

Figure 1.Comparison of 2-NBDG uptake of GLUT2-overexpressing COS-1 cells and mock-transfected COS-1 cells.

Population of COS-1 cells transfected with GLUT2 expression vector (**A-E*****) (5 cells) or vector alone (*****F-J*****) (10 cells).* **A** *and* **F,** *phase contrast images of cells.* **B** *and* **G,** *fluorescent images measured at 540-nm wavelength before loading 2-NBDG.* **C** *and* **H,** *fluorescent images measured at 540 nm 5 min after loading 200 μM 2-NBDG.* **D** *and* **I,** *net increase in the 2-NBDG fluoresecnce in cells shown as pseudocolor subtraction images. Fluorescence intensity before application of 2-NBDG was subtracted from that after its application. The* **bottom** *of the* **color scale bar** *indicates low fluorescence intensity and the top high intensity.* **E** *and* **J,** *immunocytochemistry of GLUT2. Cells were incubated with GLUT2 primary antibody and rhodamine-conjugated secondary antibody. In* **B, C, G,** *and* **H,** *cells were superfused continuously with KRB containing 5.6 mM glucose at 25°C.* **Scale bar** *is 50 μm.*

To confirm that the COS-1 cells showing strong 2-NBDG fluorescence actually expressed abundant GLUT2, the cells were immunocytochemically stained with anti-GLUT2 antibody after measurement of 2-NBDG uptake. As shown in Fig. 1E, the COS-1 cells that emitted 2-NBDG fluorescence stained with anti-GLUT2 antibody, but the control cells did not (Fig. 1J). Uptake of 2-NBDG into COS-1 cells transfected with GLUT1 or GLUT3 also was increased compared to those of mock-transfected COS-1 cells (data not shown).

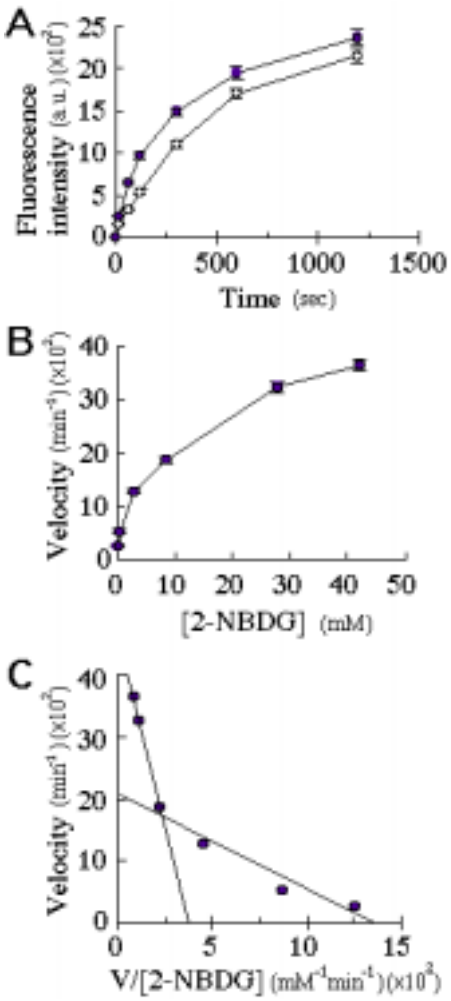

Figure 2. Kinetic analyses of 2-NBDG uptake into MIN6 cells.
A, time course of 600 μM of 2-NBDG uptake at 37°C (filled circles) and 25°C (open circles). Cells were superfused continuously with KRB. Fluorescence intensities were expressed as arbitrary units (a.u.) determined by fluorometry as described in "Experimental Procedures." Data are mean ± S.E. of 33-50 cells from an experiment representative of at least two independent experiments. B, concentration dependence of initial velocity of 2-NBDG uptake. Initial velocity of the uptake was estimated to be the difference in the fluorescence intensity before and 1 min after application of 2-NBDG at 37°C. Data are the means ± S.E. of 27-42 cells from an experiment representative of two independent experiments. C, Eadie-Hofstee plot of 2-NBDG uptake activity. Best fitted lines were drawn by linear regression analysis of the data shown in B.

To confirm that 2-NBDG is transported thorough glucose transporters, the time course and concentration dependence of 2-NBDG uptake were measured in MIN6 cells, mouse insulin-secreting clonal β-cells. MIN6 cells are known to exhibit glucose-inducible insulin secretion comparable with normal mouse islet cells, and also to express GLUT2 at a high level but GLUT1 at a barely detectable level, as do mouse pancreatic β-cells (13). The MIN6 cells were superfused with 600 μM 2-NBDG in the absence of glucose for 15 sec to 20 min at 37°C followed by washing for 5 min, and the uptake of 2-NBDG was evaluated by fluorometry. As shown in Fig. 2A, the time course was almost linear up to 2 min, and 2-NBDG fluorescence intensity at 2 min approached 43 % (mean of two independent experiments) of that at 20 min at 37°C. The initial velocity of 2-NBDG uptake into the MIN6 cells, therefore, was determined by the difference in the fluorescence intensity before and after 1-min superfusion with 2-NBDG at 37°C in the absence of glucose. It increased in a

concentration-dependent manner (Fig. 2B), and Eadie-Hofstee transformation of these data resulted in a nonlinear curve with two kinetic components, apparent Km values of 13.3 mM and 1.6 mM (Fig. 2C). 2-NBDG uptake was temperature-sensitive, and the initial velocity of the 2-NBDG uptake at 25°C was approximately half that at 37°C (Fig. 2A).

To further confirm that 2-NBDG is incorporated thorough glucose transporters, the effects of D-glucose and cytochalasin B, an antagonist of glucose transporters (4,16,17), on the uptake of 2-NBDG into MIN6 cells were examined. The cells were incubated with 600 μM 2-NBDG for 1 min in the absence or presence of various concentrations of D-glucose. 2-NBDG uptake was inhibited by D-glucose in a dose-dependent manner; it was inhibited by 37.9 ± 10.1 %, 52.5 ± 6.3 %, and 70.1 ± 7.8% (mean ± S.E. of three independent experiments) in the presence of 5.6 mM, 11.2 mM, and 22.4 mM D-glucose, respectively. Cytochalasin B was added to the medium 5 min prior to superfusion of the cells in the medium containing 2-NBDG. As seen in Fig. 3, the fluorescence intensity of the MIN6 cells that was increased after incubation with 200 μM 2-NBDG was almost completely inhibited in the presence of 10 μM cytochalasin B. These results were confirmed in six separate experiments. The increase in fluorescence intensity also was inhibited by 100 μM phloretin (data not shown).

These results demonstrate that 2-NBDG is transported into cells through mammalian glucose transporters.

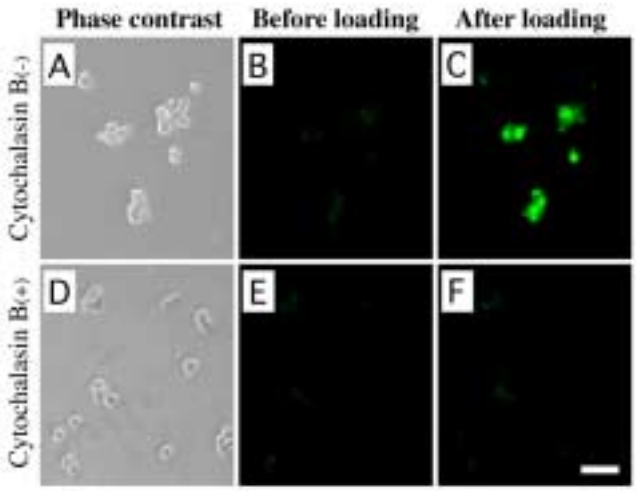

Figure 3.Effect of cytochalasin B on 2-NBDG uptake into MIN6 cells.
Clusters of MIN6 cells incubated in the absence (A-C) or presence (D-F) of 10 μM cytochalasin B are shown. A and D, phase contrast images of cells. B and E, fluorescent images measured at 540-nm wavelength before loading 2-NBDG. C and F, fluorescent images at 540 nm 5 min after loading 200 μM 2-NBDG without (C) or with (F) 10 μM cytochalasin B. In B, C, E, and F, cells were superfused continuously with KRB containing 5.6 mM glucose at 25°C. Scale bar is 50 μm.

Measurement of 2-NBDG uptake and $[Ca^{2+}]_i$ - Glucose-uptake activity and the glucose responsiveness of single pancreatic islet cells were measured. 2-NBDG was used as a tracer of glucose uptake, and changes in the $[Ca^{2+}]_i$ level in response to high glucose stimulation were monitored using fura-2 as an indicator.

A representative experiment is shown in Fig. 4. Seven of the nine islet cells showed marked increases in $[Ca^{2+}]_i$ when the extracellular glucose concentration was transiently elevated from 2.8 mM to 16.8 mM (Fig. 4, A and B, cells 1-7). The $[Ca^{2+}]_i$ of these seven cells returned to basal level upon reversal of the glucose concentration to 2.8 mM (Fig. 4B).

We then examined uptake of 2-NBDG into the same cells. The seven glucose-responsive cells emitted strong 2-NBDG fluorescence when 200 μM 2-NBDG was applied (Fig. 4, A-E, cells 1-7). On the contrary, the two other islet cells that showed no increase in $[Ca^{2+}]_i$ in response to a high concentration of glucose emitted no significant 2-NBDG fluorescence (Fig. 4, A-E, cells 8, 9). Morphologically, the cells that showed no glucose responsiveness or 2-NBDG uptake appeared somewhat smaller than the glucose-responsive cells, suggesting that the glucose-responsive cells are β-cells and the unresponsive cells are non-β-cells (18). The same cells were then characterized immunocytochemically after measurement of $[Ca^{2+}]_i$ and 2-NBDG uptake. As shown in Fig. 4F, the seven glucose-responsive islet cells stained with anti-insulin antibody (cells 1-7), but the other two cells did not (cells 8, 9), further suggesting that only the cells showing both glucose responsiveness and 2-NBDG uptake are β-cells. We confirmed that all of the 93 cells which exhibited significant rapid 2-NBDG uptake were β-cells in twelve separate experiments. Most of these cells (82 cells) exhibited an increase in $[Ca^{2+}]_i$ in response to glucose, but eleven of them did not, although they did respond to the sulfonylurea tolbutamide (0.5 mM) (data not shown).

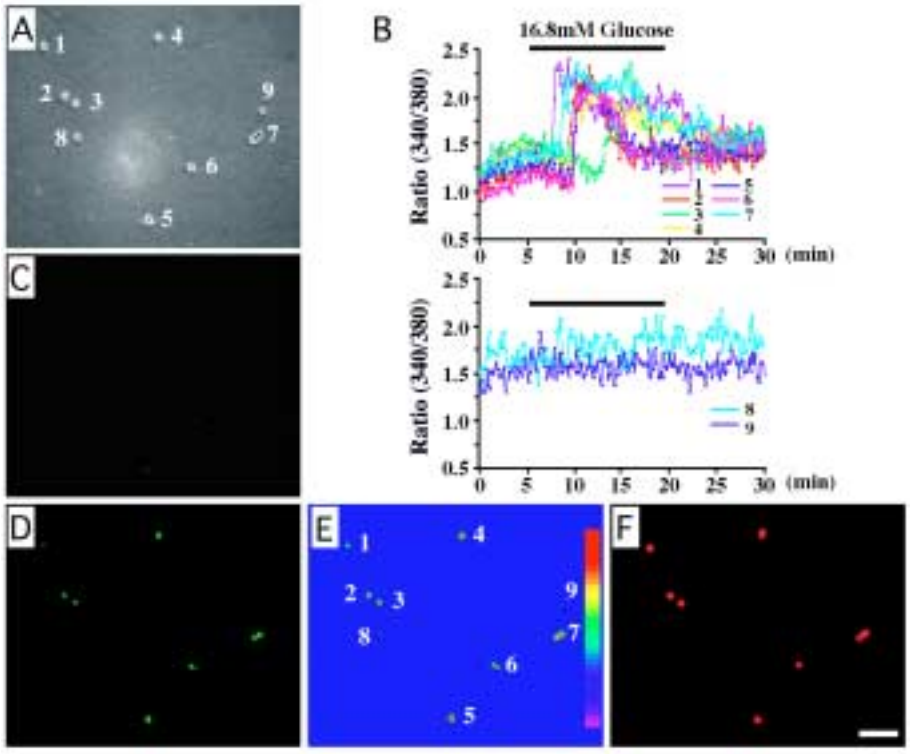

Figure 4.Measurement of 2-NBDG uptake and $[Ca^{2+}]_i$ in pancreatic islet cells.
Population of rat pancreatic islet cells (9 cells) was imaged. A, a phase contrast image. B, effects of high glucose (16.8 mM) on $[Ca^{2+}]_i$ in the islet cells. $[Ca^{2+}]_i$ responses are expressed as the change in fura-2 fluorescence ratio (340/380 nm). Horizontal bars indicate the periods of high glucose applications. C, a fluorescent image measured at 540-nm wavelength before loading 2-NBDG. D, a fluorescent image at 540 nm after loading 200 μM 2-NBDG for 1 min. E, net increase in 2-NBDG uptake into islet cells shown as a pseudocolor subtraction image. The bottom of the color scale bar indicates low fluorescence intensity and the top high intensity. F, immunocytochemistry of insulin. Cells were incubated with insulin primary antibody and rhodamine-conjugated secondary antibody. In B-D, cells were superfused continuously with KRB containing 2.8 mM glucose at 37°C; the KRB was supplemented as indicated. Numbers identify the cells in A-F. Scale bar is 100 μm.

To examine the effect of glucose metabolism on the glucose-induced $[Ca^{2+}]_i$ increase in β-

cells, DNP, an uncoupler of mitochondrial oxidative phosphorylation (15, 19), was used. A representative experiment is shown in Fig. 5. The increase in $[Ca^{2+}]_i$ in response to 16.8mM glucose was strongly inhibited in the presence of 50 μM DNP, but the responsiveness was restored after washout of DNP. The cells also responded to 0.5 mM tolbutamide, and the same cells emitted strong 2-NBDG fluorescence when 200 μM 2-NBDG was applied. These results were found in all glucose-responsive cells examined (34 cells) in five separate experiments. We also examined the effect of DNP on 2-NBDG uptake. 2-NBDG (200 μM) was applied to β-cells in the presence of 50 μM DNP, but 2-NBDG uptake into the β-cells was unaffected (five separate experiments, data not shown).

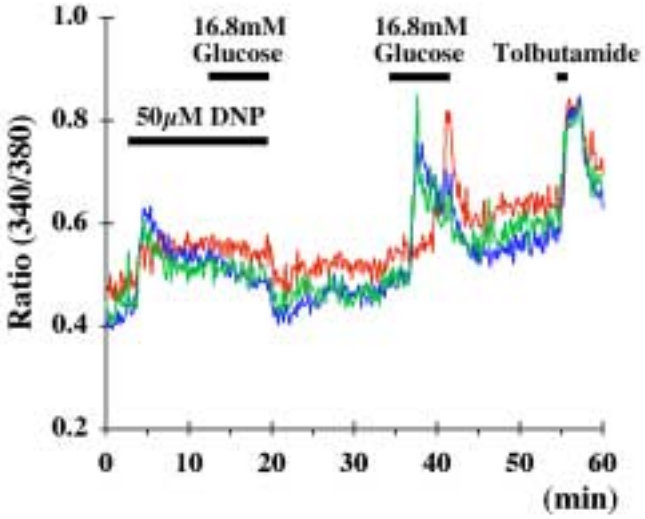

Figure 5.Effect of DNP on glucose-induced $[Ca^{2+}]_i$ change in islet cells.
Effects of high glucose (16.8 mM) and 0.5 mM tolbutamide on $[Ca^{2+}]_i$ in three islet cells in the absence or presence of 50μM DNP. $[Ca^{2+}]_i$ responses are expressed as the change in fura-2 fluorescence ratio (340/380 nm). Cells were superfused continuously with KRB containing 2.8 mM glucose at 37°C. Horizontal bars indicate the periods of DNP, high glucose, and tolbutamide applications.

To ascertain the inability of non-β-cells to incorporate 2-NBDG, an experiment with glucose and tolbutamide was performed, as shown in Fig 6. Three of the four islet cells showed a $[Ca^{2+}]_i$ increase in response to both 16.8 mM glucose and 0.5 mM tolbutamide, and incorporated significant 2-NBDG (Fig. 6, A-E, cells 1-3). The one islet cell that exhibited no $[Ca^{2+}]_i$ increase in response to either glucose or tolbutamide also did not show significant 2-NBDG uptake and was stained with anti-glucagon antibody (Fig. 6, A-F, cell 4). We performed eight separate experiments, and nine of the thirteen cells that exhibited no glucose- or tolbutamide-induced $[Ca^{2+}]_i$ increase also incorporated no significant 2-NBDG rapidly and were stained with anti-glucagon antibody. The other four cells were not stained, indicating that they are non-β–, non-α–cells such as somatostatin-secreting δ-cells or pancreatic polypeptide-secreting PP cells. In contrast, no glucose- or tolbutamide-responsive cells were stained with anti-glucagon antibody (43 cells).

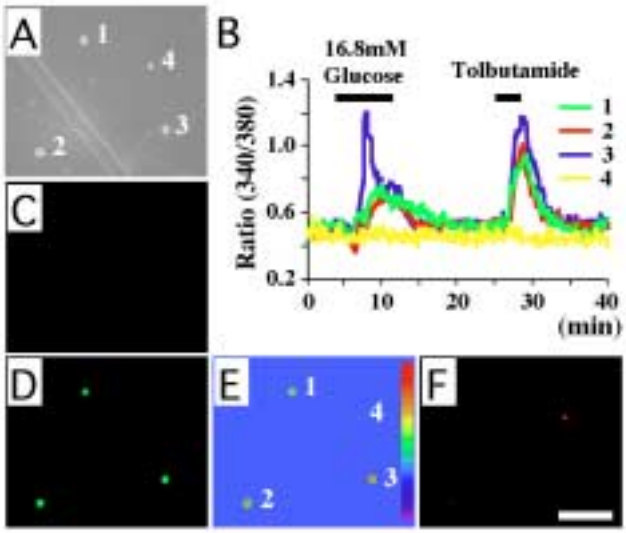

Figure 6.Characterization of glucose-unresponsive islet cells.
A population of rat pancreatic islet cells (4 cells) was imaged. A, a phase contrast image of the islet cells. B, effects of 16.8 mM glucose and 0.5 mM tolbutamide on $[Ca^{2+}]_i$ in the cells. $[Ca^{2+}]_i$ responses are expressed as the change in fura-2 fluorescence ratio (340/380 nm). Horizontal bars indicate the periods of high glucose and tolbutamide applications. C, a fluorescent image measured at 540-nm wavelength before loading 2-NBDG. D, a fluorescent image at 540 nm after loading 200 μM 2-NBDG for 1 min. E, net increase in 2-NBDG uptake into the cells shown as a pseudocolor subtraction image. The bottom of the color scale bar indicates low fluorescence intensity and the top high intensity. F, immunocytochemistry of glucagon. Only the glucose-unresponsive cell (4) was stained. Cells were incubated with glucagon primary antibody and rhodamine-conjugated secondary antibody. In B-D, cells were superfused continuously with KRB containing 2.8 mM glucose at 37°C, and the KRB was supplemented as indicated. Numbers identify the cells in A-F. Scale bar is 100 μm.

To ascertain that the non-β cells incorporate 2-NBDG after longer incubation, 2-NBDG uptake into islet cells was estimated after 10-min superfusion with 200 μM 2-NBDG. In a representative experiment, all 95 of the islet cells eventually showed 2-NBDG uptake, although there was extremely weak flouresence intensity in a small population of the cells (18 cells). We determined that 10 of the 18 cells were α-cells by staining with anti-glucagon antibody, and the average fluorescence intensity of the α-cells (379.1 ± 37.4; mean ± S.E.) was about one-tenth that of β-cells measured under the same condition (3000-6000). These results were confirmed in three independent experiments.

DISCUSSION

2-NBDG is a fluorescent derivative of D-glucose that has been modified with a 2-*N*-(7-nitrobenz-2-oxa-1,3-diazol-4-yl)amino group at the C-2 position. We have shown in previous studies that 2-NBDG is taken into the cytoplasm of both *Escherichia coli* cells and yeast *Candida albicans* cells and that it is useful for assaying viability of cells (8, 20). Uptake of 2-NBDG into these cells is inhibited by D-glucose but not by L-glucose, suggesting that it is transported into the cells through the glucose transporter system (8, 20), but this has not been determined in mammalian cells. In the present study, we have demonstrated that 2-NBDG is incorporated into mammalian cells through GLUTs. 2-NBDG was incorporated into the mouse insulin-secreting clonal MIN6 cells in a time- and concentration-dependent manner, and kinetic analysis revealed two Km components of 13.3 mM and 1.6 mM. These values are similar to those for D-glucose and the nonmetabolizable glucose analogue, 3-*O*-methyl-D-

glucose (17) found in pancreatic islets and cultured pancreatic β-cells, in which GLUT1 is expressed at low levels, whereas GLUT2 is much more abundant (21, 22). Because MIN6 cells also express GLUT1 at a very low level (13), these data suggest that the high Km and low Km correspond to the affinities of 2-NBDG for GLUT2 and GLUT1, respectively**.** Ishihara *et al*. (23) have reported that the uptake of 3-*O*-MG is rapid, and that equilibration is 80% complete in 1 min in MIN6 cells. This is comparable with the time course of 2-NBDG uptake into MIN6 cells reported in this study, although the 2-NBDG uptake is somewhat slower.

A fluorescent derivative of D-glucose, 6-NBDG, which is modified at the C-6 position, has been developed by Speizer et al. (24). They found 6-NBDG to be incorporated into human erythrocytes, but gradually to come out of the cell without any modification, probably because it does not enter the glycolytic pathway, glucose metabolism beginning with phosphorylation at the 6-hydroxyl group of D-glucose. In contrast, 2-NBDG is metabolized to a phosphorylated fluorescent derivative at the C-6 position, i.e., 2-NBDG 6-phosphate, after incorporation, and then decomposes to a nonfluorescent derivative in *Escherichia coli* cells (8, 25). Thus, the level of fluorescence intensity of 2-NBDG may be equilibrium of generation and decomposition of the fluorescent derivative. 2-NBDG fluorescence was not noticeably reduced up to 30 min after loading in this study (data not shown).

We then used 2-NBDG to evaluate glucose uptake activity together with changes in $[Ca^{2+}]_i$ in response to glucose stimulation in single, living pancreatic islet cells. It is thought that although an increase in glucose metabolism is essential for insulin secretion, the capacity for glucose uptake is very high, so transport is not rate-limiting. Gorus et al. have separated β-cells from non-β-cells by fluorescence-activated cell sorting, and shown that [^{14}C] D-glucose or 3-*O*-methyl-D-glucose is rapidly equilibrated within 2 min across the plasma membrane in β-cells at both low (600 μM) and high (20 mM) glucose concentrations (26). In contrast, they showed that intracellular [^{14}C] D-glucose or 3-*O*-methyl-D-glucose remains much lower and does not equilibrate even 30 min after incubation in α-cells. However, it has been difficult to evaluate the relationship between the glucose uptake activity and the glucose responsiveness of the cells in real time at the singe cell level. We show here that single pancreatic β-cells in which $[Ca^{2+}]_i$ increases in response to a high concentration of glucose have high 2-NBDG uptake activity. Not all of the β-cells with significant uptake of 2-NBDG exhibited an increase in $[Ca^{2+}]_i$ in response to glucose, however. These results suggest that not only glucose uptake but also the subsequent glucose metabolism plays a pivotal role in glucose-induced insulin secretion from β-cells (27). This is supported by the finding of the glucose-induced increase in $[Ca^{2+}]_i$ that is inhibited reversibly by the metabolic inhibitor DNP in β-cells, even though these cells show significant uptake of 2-NBDG. Since DNP had no effect on the 2-NBDG uptake into β-cells, it is suggested that glucose metabolism has little effect on the rapid equilibration of glucose uptake in β-cells. On the other hand, a small population of the islet cells showed no similar significant, rapid incorporation of 2-NBDG. All of these cells also lacked glucose-induced $[Ca^{2+}]_i$ responsiveness. These cells, therefore, were non-β-cells or possibly α-cells; although they eventually showed 2-NBDG uptake after longer incubation, their fluorescence intensities were much weaker than those of β-cells.

These results show that 2-NBDG is an effective tracer of glucose transport activity in pancreatic β-cells. 2-NBDG should also be helpful in clarifying the mechanisms underlying dynamic glucose uptake-function coupling in other glucose-responsive tissues and cells.

Acknowledgments **-** We are grateful to Drs. S. Seino (Chiba University) and S. Nagamatsu (Kyorin University) for the gift of GLUT2 expression vector and GLUT1 and 3 expression

vectors, respectively. We also thank Dr. J. Miyazaki (Osaka University) for providing us with MIN6 cells.

REFERENCES

1. Sokoloff, L., Reivich, M., Kennedy, C., Des Rosiers, M. H., Patlak, C. S., Pettigrew, K. D., Sakurada, O., and Shinohara, M. (1977) *J. Neurochem.* **28,** 897-916
2. Turkheimer, F., Moresco, R. M., Lucignani, G., Sokoloff, L., Fazio, F., and Schmidt, K. (1994) *J. Cereb. Blood Flow Metab.* **14,** 406-422
3. Dienel, G. A., Cruz, N. F., Adachi, K., Sokoloff, L., and Holden, J. E. (1997) *Am. J. Physiol.* **273,** E839-E849
4. Axelrod, J. D., and Pilch, P. F. (1983) *Biochemistry* **22,** 2222-2227
5. Sokoloff, L. (1993) *Dev. Neurosci.* **15,** 194-206
6. Zeller, K., Rahner-Welsch, S., and Kuschinsky, W. (1997) *J. Cereb. Blood Flow Metab.* **17,** 204-209
7. Brock, C. S., Meikle, S. R., and Price, P. (1997) *Eur. J. Nucleic. Med.* **24,** 691-705
8. Yoshioka, K., Takahashi, H., Homma, T., Saito, M., Ki-Bong, O., Nemoto, Y., and Matsuoka, H. (1996) *Biochim. Biophys. Acta* **1289,** 5-9
9. Bell, G. I., Kayano, T., Buse, J. B., Burant, C. F., Takeda, J., Lin, D., Fukumoto, H., and Seino, S. (1990) *Diabetes Care* **13,** 198-208
10. Ashcroft, F. M., and Rorsman, P. (1989) *Prog. Biophys. Mol. Biol.* **54,** 87-143
11. Inagaki, N., Gonoi, T., Clement IV, J. P., Namba, N., Inazawa, J., Gonzalez, G., Aguilar-Bryan, L., Seino, S., and Bryan, J. (1995) *Science* **270,** 1166-1170
12. Yada, T., Itoh, K., Nakata, M. (1993) *Endocrinology* **133,** 1685-1692
13. Miyazaki, J., Araki, K., Yamato, E., Ikegami, H., Asano, T., Shibasaki, T., Oka, Y., and Yamamura, K. (1990) *Endocrinology* **127,** 126-132
14. Grynkiewicz, G., Poenie, M., Tsien, R. Y. (1985) *J. Biol. Chem.* **260,** 3440-3450
15. Fujitani, S., Okazaki, K., and Yada, T. (1997) *Br. J. Pharmacol.* **120,** 1191-1198
16. Kletzien, R. F., and Perdue, J. F. (1973) *J. Biol. Chem.* **248,** 711-719
17. Johnson, J. H., Newgard, C. B., Milburn, J. L., Lodish, H. F., and Thorens, B. (1990) *J. Biol. Chem.* **265,** 6548-6551
18. Pipeleers, D. (1987) *Diabetologia* **30,** 277-291
19. Atwater, I., Dawson, C. M., Ribalet, B., and Rojas, E. (1979) *J. Physiol.* **288,** 575-588
20. Yoshioka, K., Oh, K.-B., Saito, M., Nemoto, Y., and Matsuoka, H. (1996) *Appl. Microbiol. Biotechnol.* **46,** 400-404
21. Yasuda, K., Yamada, Y., Inagaki, N., Yano, H., Okamoto, Y., Tsuji, K., Fukumoto, H., Imura, H., Seino, S., and Seino, Y. (1992) *Diabetes* **41,** 76-81
22. Heimberg, H., De Vos, A., Pipeleers, D., Thorens, B., and Schuit, F. (1995) *J. Biol. Chem.* **270,** 8971-8975
23. Ishihara, H., Asano, T., Tsukuda, K., Katagiri, H., Inukai, K., Anai, M., Kikuchi, M., Yazaki, Y., Miyazaki, J.-I., and Oka, Y. (1993) *Diabetologia* **36**, 1139-1145
24. Speizer, L., Haugland, R., Kutchai, H. (1985) *Biochim. Biophys. Acta* **815,** 75-84
25. Yoshioka, K., Saito, M., Oh, K.-B., Nemoto, Y., and Matsuoka, H., Natsume, M., and Abe, H. (1996) *Biosci. Biotech. Biochem.* **60,** 1899-1901
26. Gorus, F. K., Malaisse, W. J., and Pipeleers, D. G. (1984) *J. Biol. Chem.* **259,** 1196-

1200
27. Meglasson, M. D., and Matschinsky, F. M. (1984) *Am. J. Physiol.* **246,** E1-E13